PERMANENT MAGNETS IN MAGNETIC FIELD CALCULATIONS

H. Zijlstra
Philips Research Laboratories, Eindhoven, The Netherlands

Abstract

The presence of a permanent magnet in an electromagnetic system complicates the field calculations. The properties of the permanent magnet material that affect the calculations are analyzed theoretically. The results are tested by experiments with Ferroxdure magnets.
A magnet model characterized by four parameters can be incorporated into field calculations. The customary manufacturer's data seem to be sufficient to deal with practical systems.

Introduction

The ever increasing quality of permanent magnet materials has led to a great expansion of the area of applications. Magnets are used in loudspeakers, electric motors and generators, relays, bearings and couplings, magnetic chucks and clamps, ore separators, microwave tubes, to name only a few. In all these applications the magnet serves to generate a magnetic field in an airgap by which a mechanical force is exerted on electric conductors or on magnetizable bodies.
The desire for better performance and also the occasionally high price of the magnet materials call for optimum design of the device containing the magnet.
In the past such optimizations were made by simple calculations on crude models and by experiments. Increasing complexity, however, and seeking for the ultimate percent have created a need for more rigorous methods. In the meantime computer programs have been developed for calculating field distributions in electromagnetic systems. Such programs work satisfactorily as long as the source of magnetomotive force is an electric current and provided that isotropic soft-magnetic materials are used.
But the introduction of a permanent magnet as an MMF source is a complication and this paper attemps to contribute to the solution of the problem. In particular, we shall consider which material properties are relevant and should be supplied by the manufaturer of permanent magnets.

The Permanent Magnet

The magnetic flux density **B** in any magnetizable material can be written as

$$\mathbf{B} = \mu_0(\mathbf{H} + \mathbf{M}), \tag{1}$$

where $\mu_0\mathbf{H}$ is the contribution from the field and $\mu_0\mathbf{M}$ the contribution from the material.
For a permanent magnet **M** can be written as

$$\mathbf{M} = \mathbf{M}_0 + \chi\mathbf{H}, \tag{2}$$

where $\mathbf{M}_0$ is called the remanence and χ the susceptibility, which is a function of **H** as well.

Fig. 1 shows the first and second quadrant of a typical hysteresis loop of a permanent magnet material. This curve is known as the demagnetization curve.

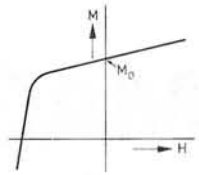

Fig. 1 Demagnetization curve of a permanent magnet material (schematic).

The permanent magnet differs from a soft magnetic material in having a magnetic moment when no magnetizing field is present. It is the magnetic moment $\mathbf{M}_0$ that serves as the source of the magnetomotive force.
Substituting **M** into **B** we obtain

$$\mathbf{B} = \mu_0(\mu_r\mathbf{H} + \mathbf{M}_0), \tag{3}$$

where we have written μ_r for $1+\chi$. Introducing the vector potential **A** by $\mathbf{B} = \text{curl}\,\mathbf{A}$ and applying the curl operator on both sides we have

$$\text{curl}\,(\mu_0^{-1}\mu_r^{-1}\text{curl}\,\mathbf{A}) = \text{curl}\,(\mu_r^{-1}\mathbf{M}_0) + \text{curl}\,\mathbf{H}. \tag{4}$$

This is the vector equation that is to be solved by the computer. This paper is limited to the discussion of μ_r or rather χ.
We consider the source term with $\mathbf{M}_0$. If we have an ideal magnet, i.e. a magnet that maintains a constant magnetic moment $\mathbf{M}_0$ in any field that might work on it, then μ_r is equal to one and a scalar. The curl of $\mathbf{M}_0$ is then zero throughout the magnet and differs from zero only at the magnet's boundary. The magnet can be considered as carrying a current sheet at its surface that generates its remanent magnetic moment. The density **j** of this current is given by

$$\mathbf{j} = \text{curl}\,\mathbf{M}_0 \tag{5}$$

or, by applying Stokes' theorem,

$$\mathbf{j} = \mathbf{M}_0{}^t, \tag{6}$$

where $\mathbf{M}_0{}^t$ is the tangential component of $\mathbf{M}_0$ at the surface and the current density **j** flows at right angles around $\mathbf{M}_0$ in a right-hand screw relation. Thus a cylindrical magnet magnetized along its axis is equivalent to a homogeneous cylindrical current sheet of a total strength $\mathbf{M}_0 l$, where l is the length of the magnet.

Now if the magnet is not ideal μ_r is greater than one and trouble may arise in several ways.

1) If μ_r depends on **H** and **H** is not uniform throughout the magnet, the equivalence of a magnet and a current sheet no longer holds.
2) If **B** and **H** have not the same orientation the curve of fig. 1 gives insufficent information, as in such curves one always measures the **B** component along the field **H**.
   For complete information curves for all combinations of **B** and **H** orientations would be required.

3) If the magnet has anisotropic μ_r matters become even more complicated, because then the orientations relative to the magnet axes have to be taken into account as well.

It will be clear that it is virtually impossible to require such information from a magnet supplier and to feed it into the program. It seems more practical to try to find a magnet model that is characterized by a few parameters and that generates the B-H curves for any combination of **B** and **H** to a good approximation of what would be found in a real experiment. To that end we shall first take a closer look into what a permanent magnet material actually is.

What is a Permanent Magnet Material?

A permanent magnet consists of many small crystallites of a highly anisotropic magnetic material. Each of these crystallites has an individual crystallographic axis along which it prefers to be magnetized, its easy axis. The crystallites are compacted to a solid body with their easy axes more or less aligned with respect to each other. The magnet thus has an average easy axis around which the local easy axes of the crystallites are oriented according to a certain distribution function. For practical purposes this function can often be approximated by assuming that the individual orientations are distributed with uniform density inside a cone with semi-apex angle Θ^*, with no orientations outside (see figure 2). The cone axis coincides with the average easy axis of the magnet.

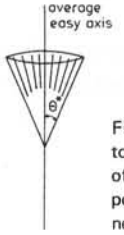

Fig. 2 First-order approximation to the distribution of easy axes of crystallites in an anisotropic polycrystalline permanent magnet.

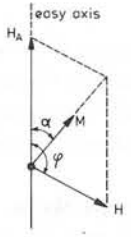

Fig. 3 Orientation of magnetization vector **M** under the combined action of the anisotropy field $\mathbf{H}_A$ and an applied field **H**.

We now consider one crystallite. It is uniformly magnetized with a magnetization $\mathbf{M}_s$ (s for saturation). The magnetization can vary under the influence of an externally applied field by two processes:

a) uniform rotation, where $\mathbf{M}_s$ maintains its modulus and only varies its orientation;

b) reversal, where $\mathbf{M}_s$ reduces its modulus to zero and grows in the reverse direction to aquire the value $-\mathbf{M}_s$.

When no field is applied $\mathbf{M}_s$ is oriented along one of the two possible directions of the easy axis. Rotation of $\mathbf{M}_s$ requires energy because of the magnetic anisotropy. The strength of the anisotropy is often expressed in terms of anisotropy field $\mathbf{H}_A$. This is a fictitious field, imagined to be oriented along the easy axis and to bind the magnetization vector to this axis. The strength of the anisotropy field is chosen such that the vector sum of an applied field **H** and the anisotropy field determines the correct orientation of $\mathbf{M}_s$ under the combined action of the anisotropy and the applied field (fig. 3). For small angles α between $\mathbf{M}_s$ and the easy axis, $\mathbf{H}_A$ can be considered as a constant field. For larger angles $\mathbf{H}_A$ has to depend on this angle, but this situation is of no practical importance to our problem; fields are always small compared to $\mathbf{H}_A$. It should be emphasized that $\mathbf{H}_A$ is a fictitious field and may not be introduced as such in a calculation. Its influence has rather to be incorporated in terms of susceptibility or permeability, as we shall see later.

Apart from the gradual rotation of the magnetization vector $\mathbf{M}_s$ under the influence of an applied field **H** another process may occur. If the applied field has a component opposite to $\mathbf{M}_s$ the latter will suddenly reverse its sign when H exceeds a certain critical value H_r, which value depends on the angle φ between **H** and the easy axis. The vector $\mathbf{M}_s$ then seeks a new equilibrium orientation under the combined action of **H** and $\mathbf{H}_A$, the latter now pointing along the easy axis opposite to its orientation before the reversal jump (see fig. 4).

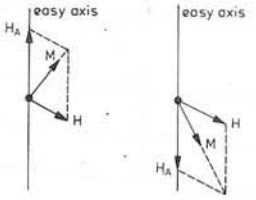

Fig. 4 Relative orientations of $\mathbf{H}_A$, **M** and **H** before (left) and after (right) a reversal jump.

This reversal of the magnetization vector is a process entirely independent of the gradual rotation. It is associated with certain processes inside the crystal initiated by the presence of lattice defects. The reversal jumps occur at field strengths that are rarely higher than 0.2 H_A and are to be distinguished from rotation jumps, which can only occur at field strengths higher than 0.5 H_A. The latter jumps are seldom of practical importance in the discussion of permanent magnets and will be ignored in the present discussion.

We have thus completely described the behaviour of one crystallite in terms of three parameters:

a) the modulus of the magnetization M_s,

b) the strength of the anisotropy field H_A,

c) the critical field H_r for reversal of M, and its dependence on the angle φ between H and the easy axis.

A real magnet is assumed to behave as the sum of its individual crystallites, with their easy axes distributed uniformly inside a cone with semi-apex angle Θ^*, and is thus characterized by four parameters.

Experimental

The behaviour of a polycrystalline magnet as described above is based, of course, on approximations and assumptions. It is worth seeing whether a magnet behaves experimentally in accordance with this scheme.

We have made samples of two different qualities of Ferroxdure (a sintered Ba- or Sr-ferrite), labeled Fxd 1 and Fxd 2. The anisotropy field of these materials is known to be about 1.7 Tesla. [1].

Fxd 1 was a commercial quality and from measurements of the remanent magnetization after magnetizing parallel and perpendicular to the easy axis, respectively, we found a value of Θ^* of about 33° and a saturation magnetization $\mu_0 M_s = 0.415$ Tesla. Fxd 2 was a laboratory sample with $\Theta^* = 15°$ and a saturation magnetization $\mu_0 M_s = 0.465$ Tesla.

Of these materials we cut small spheres with a diameter of about 3 mm.
The M vs H curves were measured using a PAR vibrating-sample magnetometer. This instrument measures the projection M_{ex} of **M** on the applied field H_{ex}.
Before each measurement the samples were magnetized in a field of 2 Tesla along the easy axis and, at zero or small field, rotated to a fixed angle Θ between externally applied field H_{ex} and easy axis. Then H_{ex} was varied and the corresponding variation of M_{ex} recorded. Two sets of curves thus obtained are shown in figs. 5 and 6.

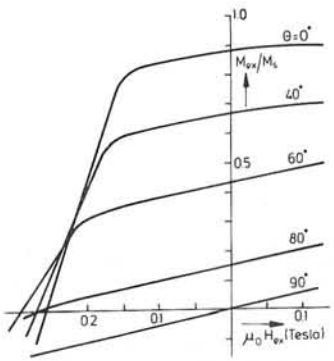

Fig. 5 M_{ex} vs H_{ex} curves of Fxd 1 spherical sample with the angle Θ between applied field H_{ex} and the easy axis as a parameter, each curve after magnetizing in a strong field along the easy axis.

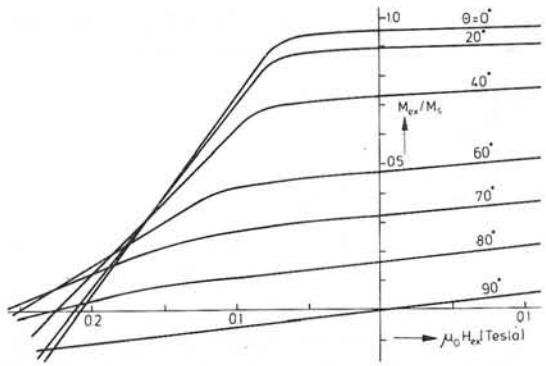

Fig. 6 As fig. 5, for Fxd 2 spherical sample.

The actual field acting upon the material is the vector sum of the applied field H_{ex} and the self-demagnetizing field H_D, arising from the poles of the sample itself (fig. 7). Only for Θ = 0 the vectors H_{ex}, H_D and **M** are parallel.

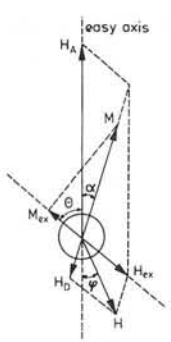

Fig. 7 Relative orientations of anisotropy field H_A, demagnetizing field H_D, applied field H_{ex}, vector sum **H** of H_{ex} and H_D, magnetization vector M, and its projection M_{ex} upon H_{ex}.

From the M_{ex} vs H_{ex} curves we derived the modulus of **M** as a function of the modulus of the total field **H** (figs. 8 and 9).

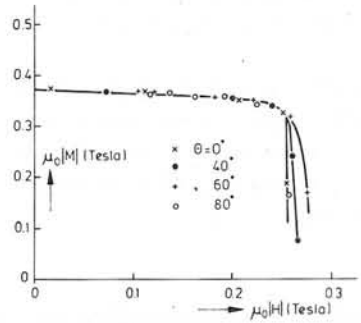

Fig. 8 Modulus of magnetization vector **M** versus modulus of total field **H**, with the angle Θ between applied field H_{ex} and easy axis as a parameter, for Fxd 1 sample.

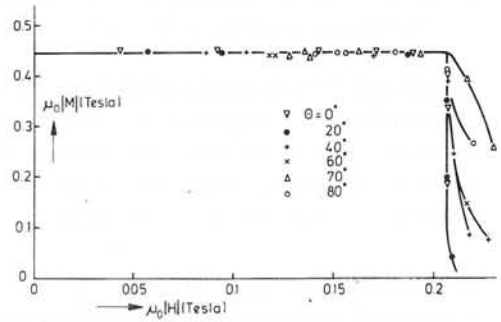

Fig. 9 As fig. 8, for Fxd 2 sample.

The curves are found to be independent of the angle Θ between H_{ex} and the easy axis, and |M| is fairly constant up to a critical value H_r where its magnitude suddenly decreases. Obviously the individual crystallite magnetizations which together add up to **M** perform small rotations in fields up to H_r, at which value the reversal process occurs. A surprising fact is that H_r is practically independent of Θ.
This notion of small reversible rotations is further supported by the observation that a sample, being in its remanent state after having been magnetized along its easy axis, conserved this state after application and removal of any field **H** with modulus smaller than H_r.
These experiments thus confirm the validity of our model.

Model for a Polycrystalline Anisotropic Magnet

The behaviour of a single crystallite can generally be described as

$$\mathbf{M} = \mathbf{M}_0 + \underline{\underline{\chi}}\,(\mathbf{H}).\mathbf{H}, \tag{7}$$

where $\underline{\underline{\chi}}$ is a non-symmetric matrix dependent on **H**.
If we take M_0 as the main axis of the description and we expand the components of M up to terms quadratic in H/H_A we obtain

$$\underline{\underline{\chi}} = \begin{vmatrix} 0 & -\frac{1}{2} M_s \frac{|H|}{H_A^2} \sin\Theta \\ -M_s \frac{|H|}{H_A^2} \sin\Theta & M_s/H_A \end{vmatrix} . \tag{8}$$

For $|H| \ll H_A$, as we assumed, the non-diagonal elements remain small with respect to M_s/H_A and may be ignored. We then have for a single crystallite

$$\underline{\underline{\chi}} = \begin{vmatrix} 0 & 0 \\ 0 & M_s/H_A \end{vmatrix} . \tag{9}$$

For an aligned polycrystalline sample we assume that the non-diagonal elements may be neglected as well, and we write

$$\underline{\underline{\chi}} = \begin{vmatrix} \chi_{/\!/} & 0 \\ 0 & \chi_{\perp} \end{vmatrix}, \qquad (10)$$

where $\chi_{/\!/}$ is the susceptibility along the easy axis and $\chi_{\perp}$ the susceptibility perpendicular to it. The spread in the individual crystallite orientations gives rise to a non-zero susceptibility along the average easy axis, but to a first approximation the contribution to the non-diagonal elements cancels out.

The usefulness of this matrix is experimentally confirmed by the agreement between a calculated and a measured M_{ex} vs H_{ex} curve for $\Theta^* = 33°$ (fig. 10).

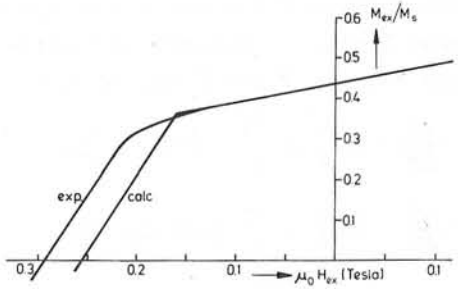

Fig. 10 M_{ex} vs H_{ex} calculated on the basis of the proposed model (see text) for $\Theta = 60°$, compared with experiment. Difference in steep part of curves is due to arbitrary choice of reversal critical field H_r in model.

Incorporation of the Model into a Computer Program

A program for computing the field distribution in electromagnet systems consisting of isotropic soft magnetic material and electrical conductors can be used for permanent magnets by simply replacing M_0 by a current sheet and ignoring any $\mathbf{M}(\mathbf{H})$. The magnet is then considered as ideal. This approach has been followed by Reichert [2] and Kamminga [3]. A refinement was introduced by Slomczynska [4], which in our context is represented by the matrix of eq. (10) with $\chi_{/\!/}$ derived from the demagnetization curve along the easy axis of the magnet, and $\chi_{\perp}$ equal to the differential susceptibility of the same curve at $H = 0$.

Polak [5] has used a somewhat different approach, with $\chi_{/\!/}$ and $\chi_{\perp}$ both equal to the value of χ derived from the demagnetization curve along the easy axis, but with $H\cos\beta$ as argument (β being the angle between B and the easy axis). Polak's model was used by Schophuizen [6] for the analysis of loudspeaker systems, who obtained the satisfactory result of only a few percent difference between calculation and measurement.

Introduction of the present model with anisotropic χ, for which not only the M-H curve parallel to the easy axis but also the perpendicular one is required, (on the understanding that initial magnetizing is done along the easy axis), might give more accurate results in more complicated designs where the magnetic vectors are expected to deviate substantially from the easy axis.

For Ferroxdure magnets, which are used in the majority of applications, knowledge of the M vs H curve perpendicular to the easy axis is not strictly required, as this curve is a straight line with slope very close to M_s/H_A, even if alignment is not so perfect (see fig. 5). Technical data provided by the manufacturer therefore suffice in giving M_s, H_A, and the M vs H curve parallel to the easy axis (the second quadrant of the hysteresis loop), which also yield H_r.

Acknowledgement

Discussions with A.J.H. Wachters have greatly contributed to this paper.

References

1 J. Smit and H.P.J. Wijn, Ferrites (Wiley, New York, 1959) p. 204
2 K. Reichert, IEEE Trans. Mag. **MAG-6**, 283 (1970)
3 W. Kamminga, J. Phys. D (Appl. Phys.) **8**, 841 (1975)
4 J. Slomczynska, IEEE Trans. Mag. **MAG-10**, 1109 (1974)
5 S.J. Polak, ISCA General **003**, 11 (1974)
6 P.J. Schophuizen, private communication

Discussion following paper:

(Jannsens, Belgium) What is your position towards the model of Stomer and Wohlfarth? This model describes a hard magnetic material by means of an assembly of ellipsoids. The magnetization curve of such an ellipsoid exhibits reversible rotation and a sudden jump. May such an approach be compared with your model?

(Zijlstra, Philips, Eindhoven) The jumps in the SW model are rotation jumps that occur only at fields greater than $0,5H_A$. The reversal jumps discussed in my paper are independent from the rotation process and occur at fields on the order of $0,1 - 0,2\ H_A$. They are associated with wall processes inside the crystal.

COMPUTATION OF MAGNETIC FIELDS IN NONLINEAR ANISOTROPIC MEDIA WITH FIELD DEPENDENT DEGREE OF ANISOTROPY

Peter Th. Weggler, CONTRAVES AG, Zurich, Switzerland

1. Summary [1]

Cold-rolled steel sheets with Goss texture are treated as nonlinear anisotropic media. Anisotropy, that is, the dependence of the permeabilities on the direction and magnitude of the vectors of the magnetic flux density $\vec{B}$ and the magnetic field strength $\vec{H}$, is fully taken into account. In the algorithm for computing the field, the magnetic properties are separated into properties for the x-direction and properties for the y-direction (≡rolling direction). On the area in question a grid with meshes of different size is applied, which can be adjusted according to the geometrical structure and the convergence properties of the problem. The vector potential is used for the representation of the magnetic field. For the determination of the vector potential at each point of the grid a two step iterative procedure of pointwise successive over-relaxation is applied. The determination of the over-relaxation factor of each grid point is based on the geometrical structure near that point and on the history of the iteration process. The values of the magnetic properties are under-relaxed. Usually different under-relaxation factors are applied for the x- and y-directions. The field lines in a 45^{o}-joint of a transformer are computed for various magnetic excitations.

2. Mathematical Formulation

Two dimensional static magnetic fields are computed. Equation (1) gives the vectorial relation between the magnetic flux density $\vec{B}$ and the magnetic field strength $\vec{H}$.

$$\vec{B} = \mu_o \cdot \| \mu_r \| (\vec{H}, \vec{B}) \cdot \vec{H} \qquad (1)$$

In this equation the relative magnetic permeability is represented by a matrix. The elements of this matrix depend on the absolute value of $\vec{B}$ and $\vec{H}$ as well as on the direction of $\vec{B}$ and $\vec{H}$ relative to the rolling direction.

$$\vec{B} = \text{curl } \vec{A} \quad (2) \qquad \text{div } \vec{A} = 0 \quad (3)$$

Equations (2) and (3) define the magnetic vector potential which is used for the representation of the magnetic field.

$$\text{curl } \vec{H} = \vec{J} \quad (4)$$

Equation (4) gives the relation between $\vec{H}$ and the distributed current densities $\vec{J}$. By applying Stokes' s theorem and equations (1,2,4) a direct relation between $\vec{J}$ and $\vec{A}$ can be derived:

$$\oint_C \left(\nu_x \cdot \frac{\partial A}{\partial y} \cdot dx - \nu_y \cdot \frac{\partial A}{\partial x} \cdot dy \right) = \iint j \cdot dx \cdot dy \quad (5)$$

$$\sum_C \left(\nu_x \cdot \frac{\Delta A}{\Delta y} \cdot \Delta x - \nu_y \cdot \frac{\Delta A}{\Delta x} \cdot \Delta y \right) = \sum j \cdot \Delta x \cdot \Delta y \quad (8)$$

$$B_x = \frac{\partial A}{\partial y} \quad (6) \qquad B_y = -\frac{\partial A}{\partial x} \quad (7)$$

ν_x and ν_y are the reciprocal permeabilities for the x- and y-directions respectively. Due to the representation of the magnetic properties the path C for computing the line integral (eq. (5)) is divided into components parallel to the x-direction and to the y-direction (≡ rolling direction). If the differential expressions in equation (5) are replaced by difference expressions, we get equation (8) which is the basis for the numerical solution of the problem.
For the determination of the vector potential $\vec{A}$ a grid divided into subsections with meshes of different size is applied on the area in question.

3. Magnetic Properties of Nonlinear Anisotropic Media [2], [3]

In ordinary soft magnetic materials the directions of the vectors of the magnetic flux density $\vec{B}$ and the magnetic field

strength $\vec{H}$ are parallel. In anisotropic materials the vectors $\vec{B}$ and $\vec{H}$ are generally not parallel to each other. Anisotropy is caused by a special crystalline structure of the material which can be obtained by means of different rolling processes and suitable annealings. Only properties of sheets with Goss texture are dealt with in this paper.

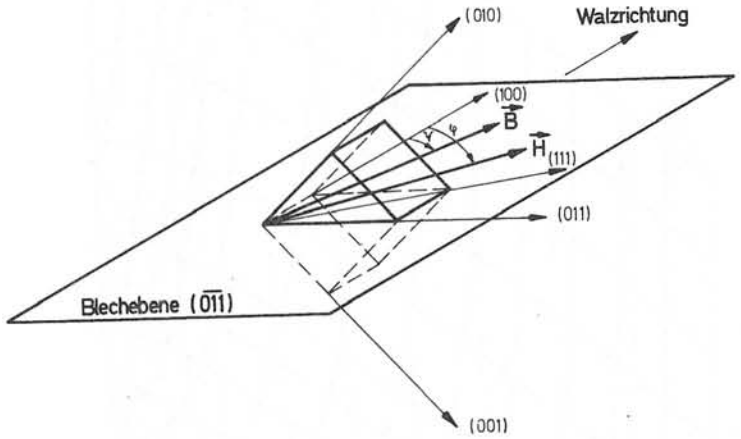

Fig. 1: Iron crystal in Goss position

Fig. 1 shows an iron crystal in Goss position. The (100)-direction is parallel to the rolling direction and represents the direction of light magnetization. The (011)-direction represents the direction of medium magnetization. The (111)-direction is the direction of strong magnetization. The (111)-direction and the (100)-direction form a n angle of about 55°. All three directions are parallel to the surface of the sheet. Ψ is the angle between $\vec{B}$ and the rolling direction. φ is the angle between $\vec{H}$ and the rolling direction.
The properties of anisotropic materials can be represented by two sets of curves. Depending on the methods of measurement result the following sets of curves.

$$|\vec{B}| = |\vec{B}\ (\vec{H})|$$
$$\Psi = \Psi\ (\vec{H}) \qquad \varphi = \text{parameter}$$

or $$|\vec{B}| = |\vec{B}\ (\vec{H})|$$
$$\varphi = \varphi\ (\vec{H}) \qquad \Psi = \text{parameter}$$

The vectors $\vec{B}$ and $\vec{H}$ can be split into components parallel to and into components perpendicular to the rolling direction (see fig. 2).

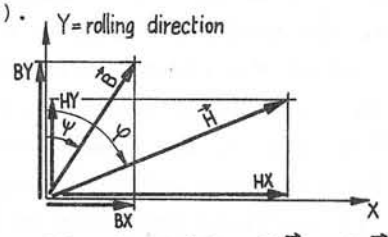

URX = HX/BX
URY = HY/BY

Fig. 2: Split of $\vec{B}$ and $\vec{H}$

The quotients URX and URY are the reciprocal values of the permeabilities in the x-direction and y-direction, provided that the y-direction is identical with the rolling direction of the sheet. Circle diagrams for $\vec{B}$ are very useful for the description of the magnetic behavior of anisotropic sheets.

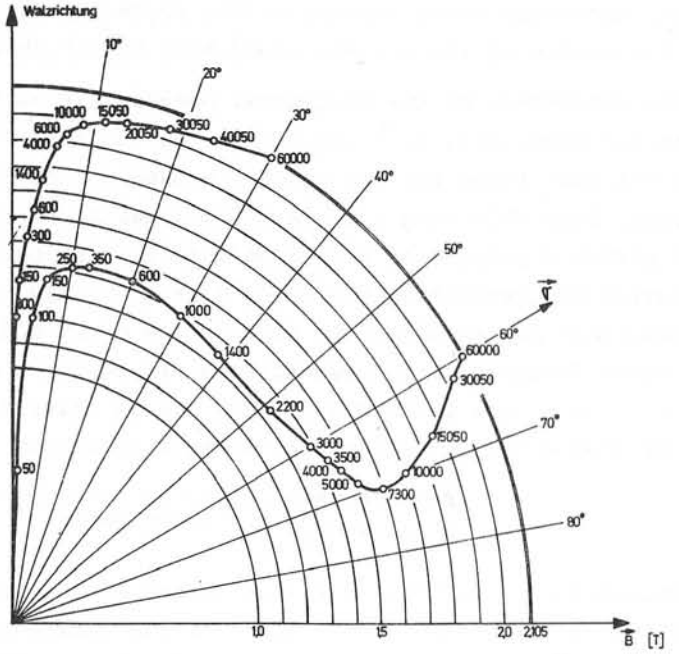

Fig. 3: Circle diagram for $\vec{B}$ for $\varphi = 30^\circ$ and $\varphi = 60^\circ$

The curves in fig. 3 show the course of the top of the vector $\vec{B}$ on the assumption that the direction of $\vec{H}$ forms fixed angles of 30° and 60° with the rolling direction and that the absolute value of $\vec{H}$ varies from zero to saturation. The figures on the curves are the absolute values of $\vec{H}$. The absolute values of $\vec{B}$ are marked in the radial direction. If the fixed direction of $\vec{H}$ forms an angle of less than 55° with the rolling direction (30° in fig. 3) the growing vector $\vec{B}$ first remains near the rolling direction and then turns towards the fixed direction of $\vec{H}$. If the fixed direction of $\vec{H}$ forms an angle of more than 55° with the rolling direction (60° in fig 3) the growing vector $\vec{B}$ first remains near the rolling direction too, but for increasing absolute values of $\vec{H}$ the direction of $\vec{B}$ turns away from the rolling direction and crosses the fixed direction of $\vec{H}$ before falling together with it. It is remarkable that the absolute value of $\vec{B}$ decreases in the area of strong angle deviation. The curves in fig. 3 are valid for sheets of the quality ARMCØ M6X, 0,014" thick.

A direct dependence of the reciprocal permeabilities (URX, URY) on the components of $\vec{B}$ (BX,BY) and on the angle Ψ respectively has been found for the algorithm used for computing the field. From this result three dimensional representations of the magnetic properties separated into properties for the x-direction and properties for the y-direction. Fig. 4 shows the reciprocal permeability URY in function of BY and Ψ. These three dimensional representations are called m a g n e t i z a t i o n s u r f a c e s. They can be calculated by means of linear interpolations in the sets of curves

$$\begin{aligned} |\vec{B}| &= |\vec{B}\ (\vec{H})| \\ \varphi &= \varphi\ (\vec{H}) \end{aligned} \qquad \Psi = \text{parameter}$$

The expression P = URX/URY is called degree of anisotropy. It is defined as the ratio between the relative permeability in the rolling direction and the one perpendicular to the rolling direction. Fig. 5 shows the shape of P in function of

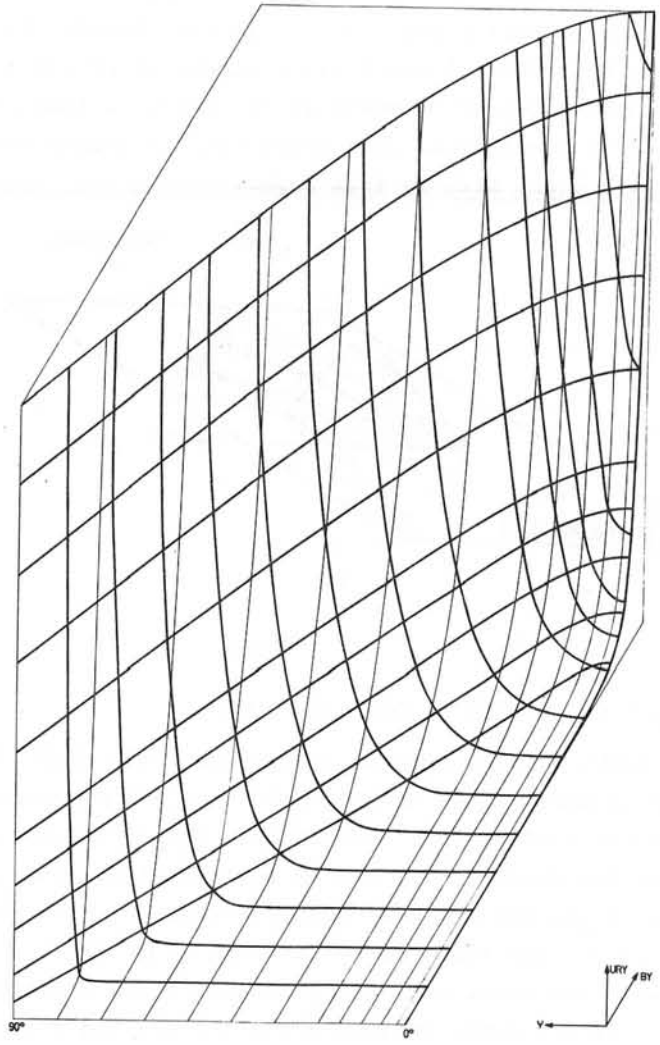

Fig. 4: Magnetization surface URY = URY (BY, Ψ)

the absolute value of $\vec{B}$ with Ψ as parameter. For $\Psi = 60^{\circ}$, 70° and 80° P can be less than 1. That means that the relative permeability perpendicular to the rolling direction is greater than the one parallel to the rolling direction.

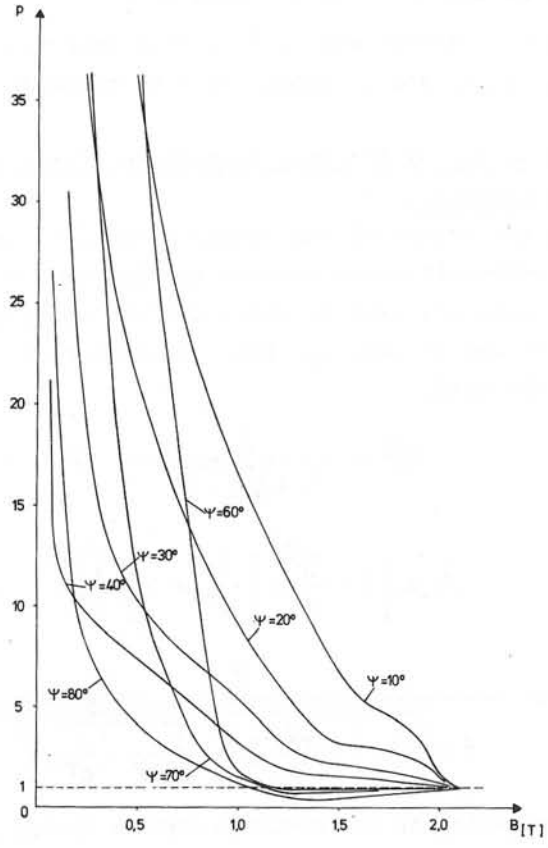

Fig. 5: Degree of anisotropy P = P ($|\vec{B}|$), Ψ

4. Numerical solution

Fig. 6 shows the meshes surrounding a certain point of the grid used for the field computation. The procedure of computation of the vector potential A (I) can be explained by means of the vector potential at point 27 in fig. 6. The diagonal which goes from point 27 to point 82 may be a boundary between two areas of iron in which the rolling directions form different angles with the y-axis of the coordinate system. Several auxiliary quantities must be determined. One of them is the vector potential AS ( ) in the centers of gravity of

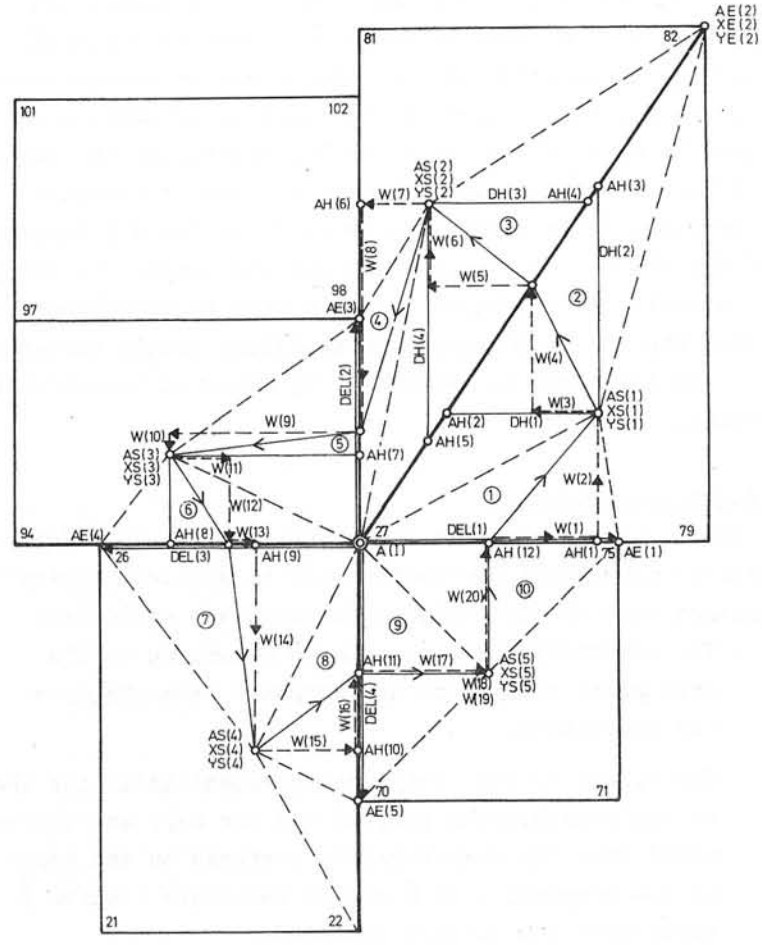

Fig. 6: Part of the grid

the rectangles or triangles, which is determined by means of the potentials on their contours. Because of the representation of the magnetic properties the path for computing the line integral (see eq. (8)) must be divided into components parallel to the x-direction and components parallel to the y-direction. (W (1) ... W (20) in fig. 6). A subdivision of the rectangles and triangles results from the position of the

centers of gravity within the rectangles and triangles and the mutual geometrical positions of the rectangles and triangles. The contours of these new basic triangles (①...⑩) caused by the subdivision are represented by dotted lines. Within such a basic triangle the magnetic properties are assumed to be constant. Crossing the boundaries the magnetic properties change discontinuously. For the determination of the permeabilities within the basic triangles the components of $\vec{B}$ for the x- and y-directions and the angle φ in the geometric centre of the basic triangle must be calculated. To do this the vector potential in auxiliary points called AH (1)... AH (12) must be calculated by means of linear interpolation.

5. Iteration procedure

For the computation of $\vec{A}$ a two step iterative procedure of pointwise successive over-relaxation is applied. During one iteration step the following operations are performed:

- The components of the vector $\vec{B}$ belonging to the grid point considered are computed from the vector potentials.
- The values of the reciprocal permeabilities for the x- and y-directions (called URX and URY) are determined from the magnetization surfaces on the basis of the components of $\vec{B}$ and of the angle φ which $\vec{B}$ forms with the rolling direction.
  Appropriate transformations are necessary if the rolling direction doesn't correspond with the y-direction of the coordinate system.
- The values URX and URY are under-relaxed by the factors FX and FY. The values of the under-relaxation factors are computed during each iteration step. They depend on the nonlinearity of the magnetization surfaces, on the over-relaxation factor for $\vec{A}$ and on the acquired relative accuracy of $\vec{A}$.
- The vector potential $\vec{A}$ is then computed with a line integral and is generally over-relaxed.

6. Determination of the over-relaxation factor for the vector potential

As a rule the values of the vector potentials are over-relaxed. Two over-relaxation factors are defined. The first one called WF (see eq. (9)) is valid for the whole grid. The second one called WL (see eq. (11)) is different at every point of the grid.

$$WF = \frac{2}{1+\sqrt{1-\lambda}} \qquad (9)$$

$$\lambda = \left[1 - \frac{\pi^2}{4} \cdot \left[\frac{1}{P^2} + \frac{1}{Q^2}\right]\right]^2 \qquad (10)$$

$$WL = \frac{2}{1+\sqrt{1-\left[1-S^2+2S^2\cdot\sqrt{\frac{1}{WF}-\frac{1}{WF^2}}\right]^2}} \qquad (11)$$

The determination of the over-relaxation factor WF (see eq. (9)) for the whole grid is based on an average mesh and on the theory for the computation of linear fields. P and Q are expressions for the number of average meshes in the x- and y-directions respectively. For the determination of the local over-relaxation factor WL (see eq. (11)) a quantity S must be found which relates the specific geometrical configuration in the vicinity of a certain point to the geometrical configuration of the whole grid. During the iteration procedure the values of WF and WL are adjusted to the convergence.

7. Determination of the under-relaxation factor for the reciprocal permeabilities

The values of the reciprocal permeabilities (URX, URY) are under-relaxed.

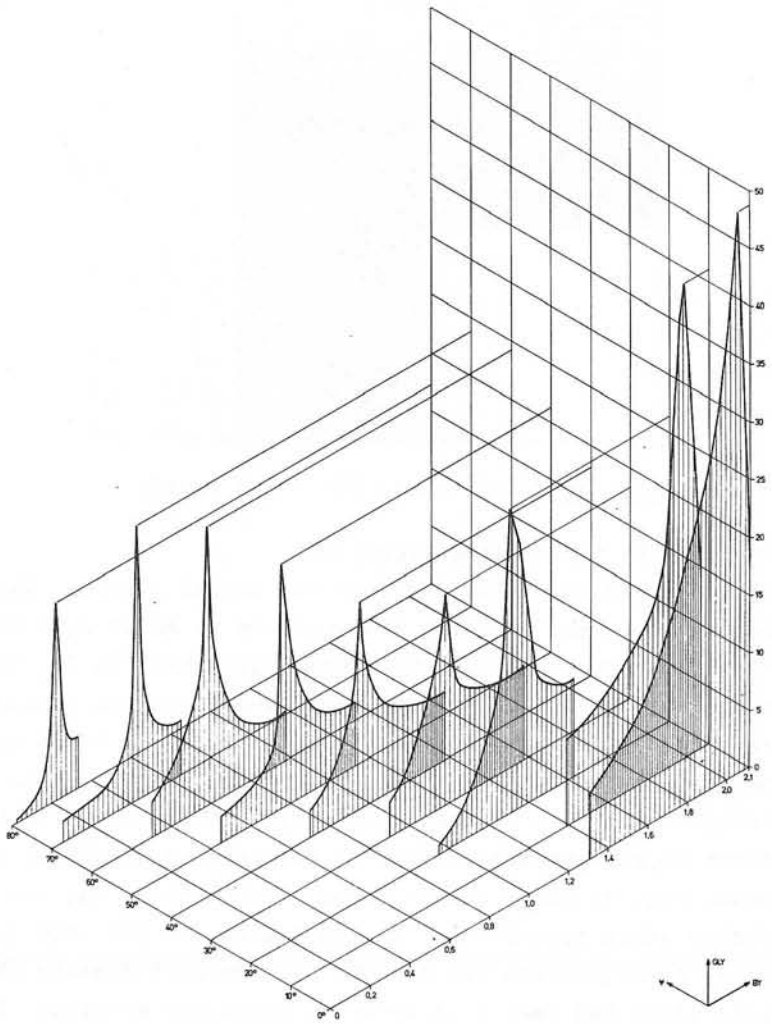

Fig. 7: Nonlinearity GLY = GLY (BY), Ψ

Usually different under-relaxation factors (FX, FY) are applied for each point of the grid and for the x- and y-directions at each point (see eq. (12, 13)).

$$FX = \frac{WL - \beta}{\beta \cdot GLX} \quad (12) \qquad FY = \frac{WL - \beta}{\beta \cdot GLY} \quad (13)$$

$$GLX = \frac{\partial URX}{\partial BX} \cdot \frac{BX}{URX} \quad (14) \qquad GLY = \frac{\partial URY}{\partial BY} \cdot \frac{BY}{URY} \quad (15)$$

The values of the under-relaxation factors depend on the nonlinearity of the magnetic surfaces (GLX, GLY; see eq. (14, 15)), on the values of the local over-relaxation factors WL and on the acquired relative accuracy of A. β is a weight for the correction of the value of the reciprocal permeabilities and depends on the acquired relative accuracy of A and on the over-relaxation factor WL. Fig. 7 shows the nonlinearity GLY for the y-direction in function of BY for different values of Ψ. The values of the under-relaxation factors are computed during each interation step.

8. Computed examples

A 45°-joint of a transformer has been chosen as an example. Fig. 8 shows the grid used for the computation for two examples. The iron boundary is marked by fat lines. The rolling direction of the sheet is marked by arrows. The current regions are marked by 1 and 2. The meshes are large in the yoke and in the limb and smaller near the joint. The values for the reciprocal permeabilities correspond with the properties of sheets of the type UNISIL 51.

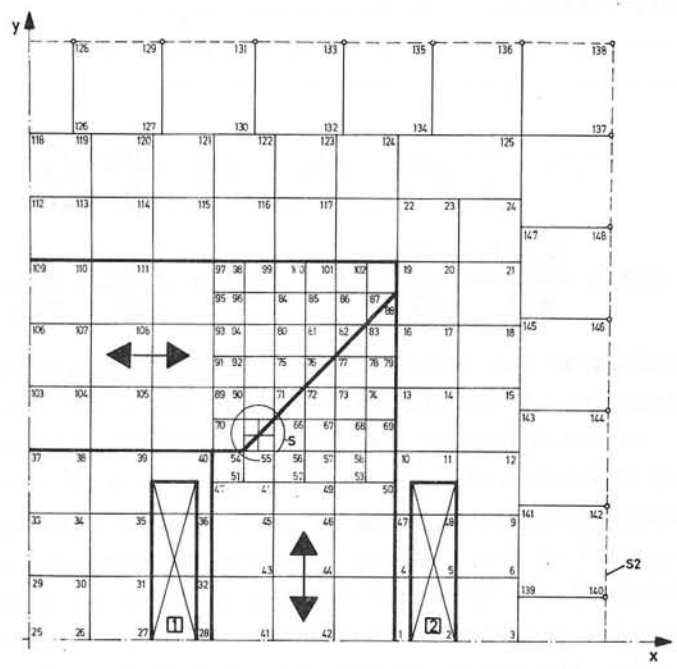

Fig. 8: Grid

The properties of the anisotropic material become evident especially with small values of the magnetic flux density. Fig. 9 shows the field lines of the first example. The average value of the magnetic flux density is about 0.9 Teslas. The relative accuracy of the vector potentials is about 10^{-4}. To get this result about 1600 iteration steps had been necessary. In the yoke as well as in the limb the field lines run almost parallel to the rolling direction. In the joint the field lines bend almost perpendicularly. This behavior has been proved by means of experiments with iron powder [4] . A compression of field lines can be observed near the inner iron boundary of the yoke, which indicates a concentration of flux. In the joint the flux distribution changes considerably. In the limb the main part of the flux runs in the middle. Only a small part of the flux in the yoke is forced to run perpendicularly to the rolling direction.

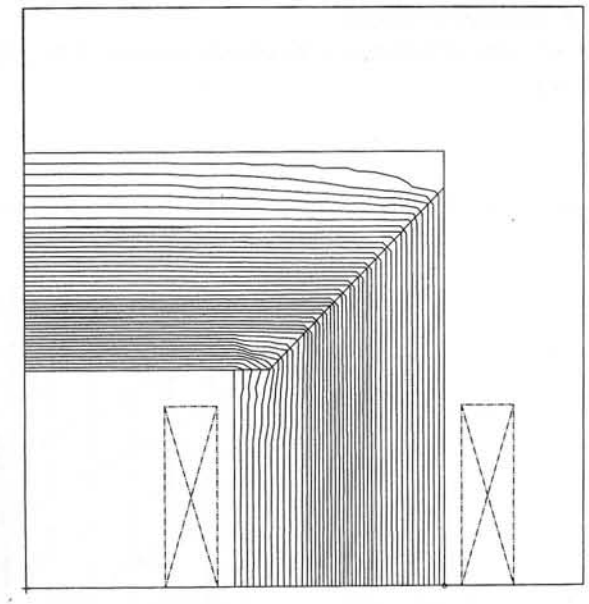

Fig. 9: Field lines; $|\vec{B}|$ = 0.9 Teslas

Fig. 10 shows the field lines of the second example. The average value of the magnetic flux density is about 1.75 Teslas. The relative accuracy of the vector potentials is $7 \cdot 10^{-5}$. To get this result about 1350 iteration steps had been necessary. In the vicinity of the junction the field lines in the yoke are displaced from the inner iron boundary towards the middle of the yoke. Thereby the part of the flux which is forced to run perpendicularly to the rolling direction is reduced. Fig. 11 shows the B-vectors (fat arrows) and the H-vectors (thin arrows) near the junction. For the same geometrical configuration and for the same current density the field lines had been calculated in isotropic material. If the two plots are laid one upon the other something like interference lines (see fig. 12) result. They clearly show the difference in the shape of field lines in anisotropic and isotropic material.

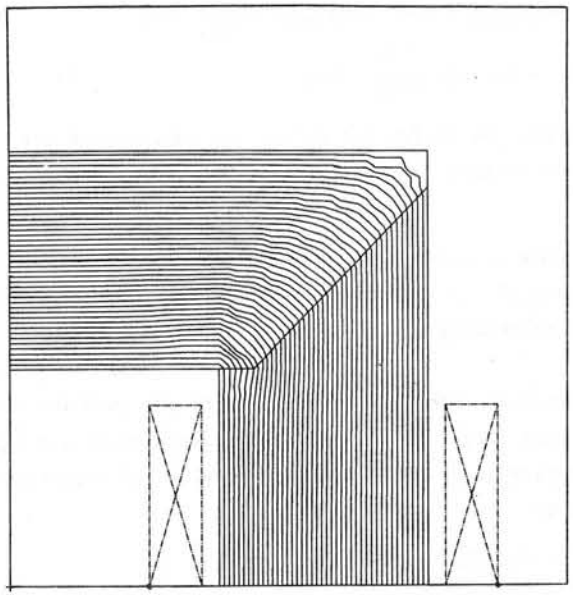

Fig. 10: Field lines; $|\vec{B}|$ = 1.75 Teslas

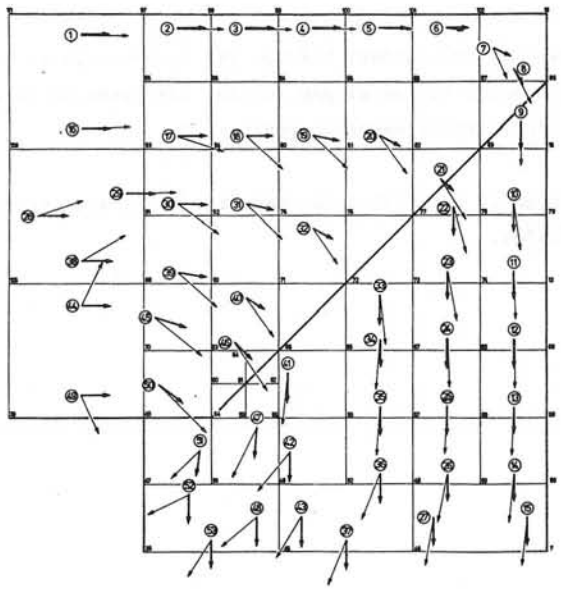

Fig. 11: B -and H-vectors

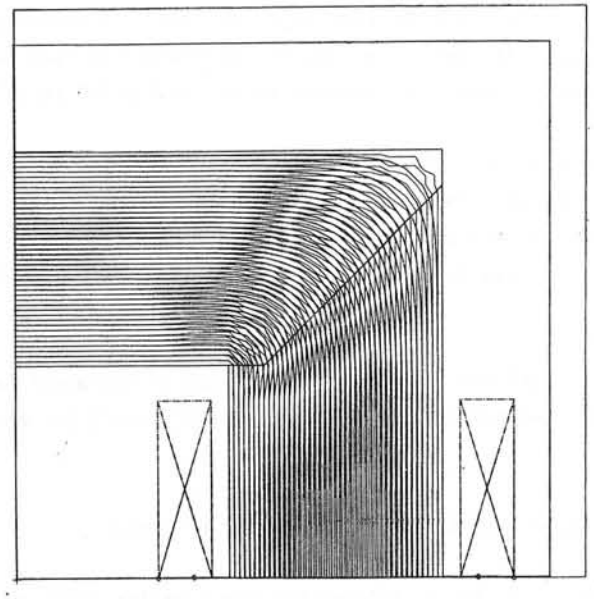

Fig. 12: Interference lines

References

[1] Weggler Peter Th.: "The computation of magnetic fields in nonlinear anisotropic media with field dependent degree of anisotropy". Thesis 5119/1973, Swiss Federal Institute of Technology.

[2] Fasching, G.M. and H. Hofman: "Messeinrichtung für anisotrope Elektrobleche". Archiv für techn. Messen und industr. Messtechnik (ATM) 1969 R57 - R68, Lieferung 400

[3] Gibler, F.: "Das magnetische Verhalten mechanisch beanspruchter anisotroper Ferromagnetika". Diss. TH. Wien, 1967.

[4] Fasching, G.M., H.Hofman und M. Schückher: "Die magnetische Bezirksstruktur in der Umgebung eines Diagonalschnittes". Elektrotechnik und Maschinenbau 68 (1969), 41-44.

Discussion following paper:

(Lord, Cardiff) Has your approach been extended to 3 dimensions? In practice the joints are overlapped and the flux moves in (and out) to the next lamination - hence the problem is inherently 3-D in nature.

(Weggler, Contraves AG) The problem is solved only for two dimensions. The airgap in the joint is assumed to be extremely small. The part of flux which moves in (and out) to the next lamination depends on the geometry of the air gap as well as on the flux density and is not taken into account.

(Phemister, C.A. Parsons) I should be grateful if you would say something about the measurement of the angle between $\underline{B}$ and $\underline{H}$ for various directions.

(Weggler) Please consult the references in my paper.

(Polak, Philips) Could you tell us why the formulas shown were used for the computation of the different under relaxation factors.

(Weggler) A basic five point representation of a grid point is assumed. For each point of the grid a residuum R can be defined:

$$R = \iint j \cdot dF - (By_1 . \nu y_1 - Bx_1 . \nu x_1 \text{ ----- } + By_4 \nu y_4)$$

$$\Delta R = -\Delta By_1 . \nu y_1 - By_1 . fy_1 . \Delta \nu y_1 + \Delta Bx_1 . \nu x_1 + \text{-----}$$

$$-\Delta By_4 . \nu y_4 - By_4 . fy_4 . \Delta \nu y_4$$

fx_i = under-relaxation factor for νx_i

fy_i = under-relaxation factor for νy_i

$$\Delta R . \alpha = (\Delta R_A + \Delta R_{UR}) . \beta \qquad (1)$$

α = local over-relaxation factor for $\vec{A}$

β = weights for the indirect correction.

Direct correction:

$$\Delta R_A = -\Delta By_1 . \nu y_1 + \Delta Bx_1 . \nu x_1 + \text{-----} -\Delta By_4 . \nu y_4 . \qquad (2)$$

Indirect correction:

$$\Delta R_{UR} = - By_1 . fy_1 . \frac{\partial \nu y_1}{\partial By_1} . \Delta By_1 + Bx_1 . fx_1 . \frac{\partial \nu x_1}{\partial Bx_1} . \Delta Bx_1$$

$$+ \text{-----} - By_4 . fy_4 . \frac{\partial \nu y_4}{\partial By_4} . \Delta By_4 \qquad (3)$$

If Eq. (2) and (3) are put in Eq. (4) we get the expressions for the under-relaxation factors fx_i and fy_i for the x - and y - directions.

(Endo, Japan) How to control the under-relaxation factors of transverse directions separately? I think it is difficult to control them for large "degree of anisotropy".

(Weggler) Different under-relaxation factors are used for the x- and y- direction. They depend on the over relaxation factor for $\vec{A}$ and on the relative accuracy of $\vec{A}$. The non linearity of the magnetic surfaces can be described by

$\frac{\partial Vx}{\partial Bx} . \frac{Bx}{Vx}$ for the x- direction and by

$\frac{\partial Vy}{\partial By} . \frac{By}{Vy}$ for the y- direction.

(Zijlstra) In practice the contact between the iron sheets is not perfect. What influence has an airgap, which, even when it is small, must represent a considerable magnetic resitance?

(Weggler) An airgap is a considerable magnetic resistance especially at low magnetic fields.

Field Computation of Magnet made of Steel with Magnetic Anisotropy

T. Kasuga, E. Takasaki, A. Ando, M. Kihara and K. Endo

National Laboratory for High Energy Physics
Oho-machi, Tsukuba-gun, Ibaraki, Japan

Abstract

The grain oriented low carbon steel has been developed for the magnet core material of the proton synchrotron and proved to have superior magnetic properties when used properly. The grain orientation brings on the magnetic anisotropy which often leads to the different results against expectations. In order to get the clear view about the field properties of the quadrupole magnet made of the grain oriented steel, computations were carried out numerically by solving a set of difference equations on the square meshes of two dimensions. Computations were tried on the models with different orientations of magnetic anisotropy and compared with the magnetic field measurements on the full scale model magnets. In accordance with the experimental results, the marked differences were obtained for the different orientations of the grain.

§1. Introduction

Since an alternating gradient principle has been applied to a circular high energy particle accelerator, the weight of the magnet has been saved greatly. This advantage, however, requires higher quality of the magnetic field than ever met, in both bending and focusing fields. As inhomogeneities in the magnetic field will cause an undesirable effect on the beam behavior, the magnet should maintain good field configuration over the required aperture during the whole of an accelerating cycle. Steel for the iron core of the accelerator magnet has to be choosed carefully from the magnetic requirement such as low coercivity with small spread and high permeability with small spread at both low and high inductions. In addition to these magnetic properties, is also required good machinability to allow the precision stamping under the clearance of 0.02 mm or less. From these points of view, low silicon steel and low carbon steel have been used. These two kinds of steel show almost the same isotropic magnetic properties except that permeability is higher for low carbon steel.

On the other hand, iron in high purity form has superior magnetic properties in itself at both low and high fields, though its production needs very careful heat treatments for reduction of the harmful nonmetalic impurities such as carbon and nitrogen which cause magnetic aging. And contents of carbon and nitrogen may be readily 0.003 and 0.005 %, respectively. Coercive force of this decarburized steel lowers remarkably by grain-growing treatment. During this grain-growing process which consists of cold rolling and hot annealing, anisotropy of the magnetic properties is developed. Permeability in the preferred direction raises and coercive force lowers appreciably without changing an ultimate saturation limit. The orientation of each grain in iron with preferred texture is within about 3 degrees to the rolling direction —— (110)[001] textured iron. This type of steel is called as grain oriented (low carbon) steel.

Grain oriented steel has very large permeability to the direction of easy magnetization in accordance with the rolling direction, while its transverse has lower permeability. The merit of using grain oriented steel as the core material for the magnet of the proton synchrotron has been tested on the full scale models of the gradient dipole magnet.[1] If the rolling direction of steel is aligned in the pole of the magnet to be perpendicular to the median plane in the air gap, the field quality is improved very much at high field. The same results were obtained from the calculations with an aid of the SIBYL program by assuming that permeability was isotropic one taken to the direction perpendicular to the median plane throughout the iron core. This assumption was based on the computational result that the flux lines inside the magnet pole was almost perpendicular to the median plane.

In the case of the quadrupole magnet, however, the magnetic properties of both transverse directions of steel have a role on the field in the air gap. Therefore, the same assumption must be avoided on this case, despite that the field computations were carried out by assuming the isotropic magnetic properties in the previous report[2] and showed the need for more detailed study to take the magnetic anisotropy of steel into consideration. First trial towards this problem was to take account of the directional dependence of the B-μ relation which was obtained experimentally.[3] This approach is rather easy because the B-μ relation to any direction can be calculated from the interpolation of the experimental data. This approach assumes the coincidence of the directions of the magnetic field and the magnetization. In general, these two directions do not coincide except for the direction of the easy magnetization. This indicates the second approach which treats permeability as a tensor quantity. In the case, the difference equations solving the vector potential in iron must be altered to deal with the tensor permeability. In this manuscript, both treatments are described

and tried by modifying the relaxation program LINDA.

§2. Computation of vector potential in anisotropic iron

For convenience of the computation, the air and iron regions are treated separately in two dimensions. That is, the magnetic field is treated by the modified scalar potential in the air and by the vector potential in the iron region both in square meshes. The computation mainly concerns with the iron region and the magnetic anisotropy is brought in the process of solving the vector potential field in iron.

2-1. Non-tensor form

An attempt to introduce the grain orientation effect into the field computation was undertaken by taking account of the directional dependence of the B-H characteristics shown in Fig.1 which were obtained by the Epstein test.[4] In the iron region where current does not exist, the Poisson equation describing the vector potential $\vec{A}$ (0, 0, A) is transformed to

$$\nabla^2(\gamma A) = 0 \quad , \tag{1}$$

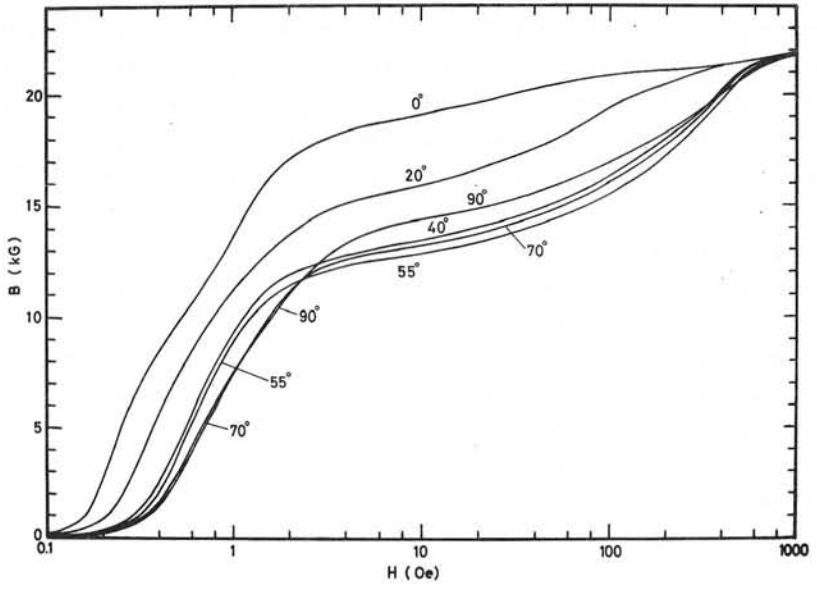

Fig.1 The B-H relation of the grain oriented steel. Figures mean the angles made by the rolling direction and the direction of the magnetizing force.

if the average reluctivity γ, reciprocal of permeability, is assumed between the adjacent mesh points.

Solving a set of the finite difference equations of eq.(1) by the successive over-relaxation method, components of the flux density at each mesh rectangle, B_x and B_y, are obtained from

$$\vec{B} = \nabla \times \vec{A} \quad . \tag{2}$$

Therefore, the direction of the flux line is given by

$$\theta = \tan^{-1} \left|\frac{B_y}{B_x}\right| = \tan^{-1} \left|\frac{dA}{dx} \Big/ \frac{dA}{dy}\right| \tag{3}$$

and the field strength by

$$H = \sqrt{H_x^2 + H_y^2} = \gamma\sqrt{B_x^2 + B_y^2} \quad . \tag{4}$$

Thus, the new γ is obtained by the linear interpolation between the input data of $B^2 - \gamma$ relations of both transverse directions, rolling and its perpendicular taken in the plane of the lamination.

In this treatment, the flux density along the direction with the angle θ with respect to the rolling direction at the field strength H can be represented as

$$B = (B_L(H) \cos^2\theta + B_C(H) \sin^2\theta)\, f(\theta, H) \quad , \tag{5}$$

where $B_L(H)$ and $B_C(H)$ stand for the flux density along the rolling direction and its transverse, respectively. An analytic function $f(\theta, H)$ is determined to reproduce the experimental B-H relations.[5]

By using new γ values in every iteration cycle, the whole process in the iron region is repeated until the change in reluctivity per cycle become below a specified value for all mesh rectangles.

2-2. Tensor form

If the tensor quantity of permeability is given by ${}^2\mu$, the flux density is

$$\vec{B} = {}^2\mu\, \vec{H} \tag{6}$$

where

$${}^2\mu = \begin{pmatrix} \mu_{11} & \mu_{12} \\ \mu_{21} & \mu_{22} \end{pmatrix} ,$$

$$\vec{B} = \begin{pmatrix} B_x \\ B_y \end{pmatrix} \quad \text{and} \quad \vec{H} = \begin{pmatrix} H_x \\ H_y \end{pmatrix} \quad . \tag{7}$$

In order to satisfy the symmetry for the rotation of the coordinates, tensor must be diagonal, that is,

$$ {}^2\mu = \begin{pmatrix} \mu_x & 0 \\ 0 & \mu_y \end{pmatrix} , \qquad (8) $$

when the direction of the easy magnetization coincides with the axis of the coordinate. If μ_x refers to permeability in the direction of rolling, μ_y is taken to be its transverse. Tensor of reluctivity ${}^2\gamma$ is obtained from the relation

$$ \gamma_{ik} = \frac{1}{|{}^2\mu|} \frac{\partial |{}^2\mu|}{\partial \mu_{ki}} . \qquad (9) $$

Then,

$$ {}^2\gamma = \begin{pmatrix} \frac{1}{\mu_x} & 0 \\ 0 & \frac{1}{\mu_y} \end{pmatrix} = \begin{pmatrix} \gamma_x & 0 \\ 0 & \gamma_y \end{pmatrix} . \qquad (10) $$

Using these expressions, the Poisson equation in the iron region is expressed as follows,

$$ \frac{\partial}{\partial x} \left(\gamma_y \frac{\partial A}{\partial x} \right) + \frac{\partial}{\partial y} \left(\gamma_x \frac{\partial A}{\partial y} \right) = 0 . \qquad (11) $$

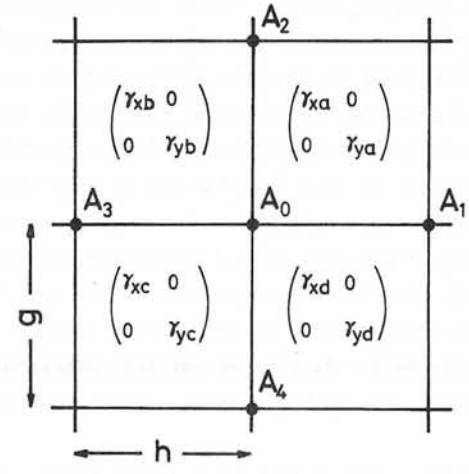

Fig.2 Tensor reluctivity in each mesh rectangle to derive the finite difference equation.

In the mesh rectangles shown in Fig.2, the finite difference equation of eq.(11) is given by

$$ \frac{\gamma_{ya} + \gamma_{yd}}{h^2} A_1 + \frac{\gamma_{xa} + \gamma_{xb}}{g^2} A_2 + \frac{\gamma_{yb} + \gamma_{yc}}{h^2} A_3 + \frac{\gamma_{xc} + \gamma_{xd}}{g^2} A_4 - 4\left(\frac{\bar{\gamma}_y}{h^2} + \frac{\bar{\gamma}_x}{g^2} \right) A_0 = 0 , \qquad (12) $$

where γ_x and γ_y in each mesh rectangle are expressed by adding suffixes (a,b,c and d) as shown in Fig.2, and

$$ \bar{\gamma}_x = \frac{1}{4} (\gamma_{xa} + \gamma_{xb} + \gamma_{xc} + \gamma_{xd}) $$

$$ \bar{\gamma}_y = \frac{1}{4} (\gamma_{ya} + \gamma_{yb} + \gamma_{yc} + \gamma_{yd}) . \qquad (13) $$

h and g are the horizontal and vertical mesh sizes, respectively. If permeability is isotropic, that is, $\gamma_x = \gamma_y$ ($\equiv \gamma$), eq.(12) becomes the difference equation of the ordinary isotropic problem,

$$ \frac{\gamma_a + \gamma_d}{h^2} A_1 + \frac{\gamma_a + \gamma_b}{g^2} A_2 + \frac{\gamma_b + \gamma_c}{h^2} A_3 + \frac{\gamma_c + \gamma_d}{g^2} A_4 - 4\bar{\gamma}\left(\frac{1}{h^2} + \frac{1}{g^2} \right) A_0 = 0 , \qquad (14) $$

where

$$ \bar{\gamma} = \frac{1}{4} (\gamma_a + \gamma_b + \gamma_c + \gamma_d) . \qquad (15) $$

In order to solve eq.(12), the initial values of γ_x and γ_y are assumed to be 0.0002. After every iteration, angles given by eq.(3) are calculated at all meshes and new reluctivities of both transverse directions are recalculated by the linear interpolation of $B_x^2 - \gamma_x$ and $B_y^2 - \gamma_y$ tables which are obtained experimentally. The problem is likely to diverge unless the iterative increments or decrements of reluctivities of both directions are limited each other. Among several trials, limitations such as

$$\langle \Delta\gamma_x \rangle = \frac{\beta |\Delta\gamma_x \cdot \Delta\gamma_y|}{(|\Delta\gamma_x| + |\Delta\gamma_y|)^2} \Delta\gamma_x$$

$$\langle \Delta\gamma_y \rangle = \frac{\beta |\Delta\gamma_x \cdot \Delta\gamma_y|}{(|\Delta\gamma_x| + |\Delta\gamma_y|)^2} \Delta\gamma_y \qquad (16)$$

seems to be good. $\Delta\gamma_x$ and $\Delta\gamma_y$ are the changes of the transverse reluctivities at some mesh rectangle after iteration and β is the under-relaxation factor. The problem converges very slow, so the iteration cycles are limitted to a few hundreds.

After computation of the iron region, the vector potential is transformed to the scalar potential to get the scalar boundary values on the air-iron interface. Changes of the scalar potential along the horizontal and vertical mesh lines are given by $-\int \gamma_x \frac{\partial A}{\partial y} dx$ and $\int \gamma_y \frac{\partial A}{\partial x} dy$, respectively. If the scalar potential is obtained according to these integrals, the boundary conditions at the air-iron interface are satisfied in the following iterative relaxation in the air region.

§3. Field problems and their results

At the medium field level for which permeabilities of both transverse directions are expected to be very high, the field distribution in the air gap is mainly determined by the shape of the pole profile. So, the design calculations on the quadrupole magnet for the lattice forcusing element to be used in the main ring of KEK proton synchrotron were carried out regardless of the magnetic anisotropy. Fig.3 shows the pole profile and the cross-sectional view of the quadrupole magnet. The rolling direction of the grain oriented steel was selected to be perpendicular to the horizontal median plane. The magnet of this type is referred as the vertically oriented one. In the same meaning, the horizontally oriented one means that the rolling direction is parallel to the horizontal median plane. The full scale models of both types were made of the laminated steel with the magnetic anisotropy shown in Fig.1. Thickness of the lamination is 1 mm.

Magnetic field was computed for the asymmetric configuration of Fig.3, although the pole profile underwent the slight modification so as to correct the field quality at the high field by using the experimental data on the full scale models. The field quality deteriorates due to the saturation

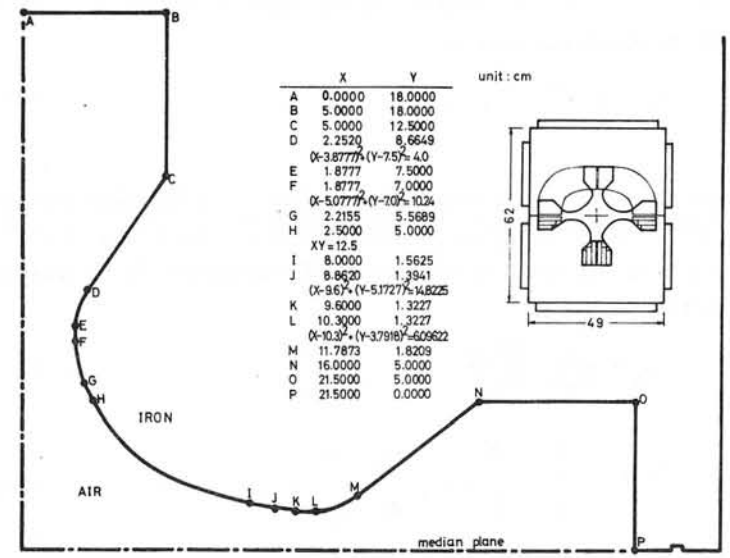

Fig.3 The pole profile and the cross-sectional view of the quadrupole magnet.

around the minimum gap on the horizontal median plane where the flux density in iron becomes high, say about 19 kG at the maximum excitation level. While the field distribution on the vertical axis does not deteriorate, because the flux density at the nose of the pole is not so high.

Fig.4 and 5 give the computational results for the vertically and horizontally oriented magnet, respectively. Also, are shown the experimental data[6] whose accuracy is ±0.1 % by the search coil method. The difference between two approaches is evident for the horizontal distribution of the vertically oriented case (Fig.4) and the tensor approach fits in the experimental data well. For the horizontally oriented case (Fig.5), however, they give the similar distributions of the field gradients and explain the experimental data fairly well. As for the vertical distributions, the difference between the computation and the magnetic field measurement is very small in two cases.

To compare the grain oriented cases with the non-oriented case, the quadrupole magnet with the same size was made of the low silicon steel and its field was measured. Fig.6 contains the results of the experiment and

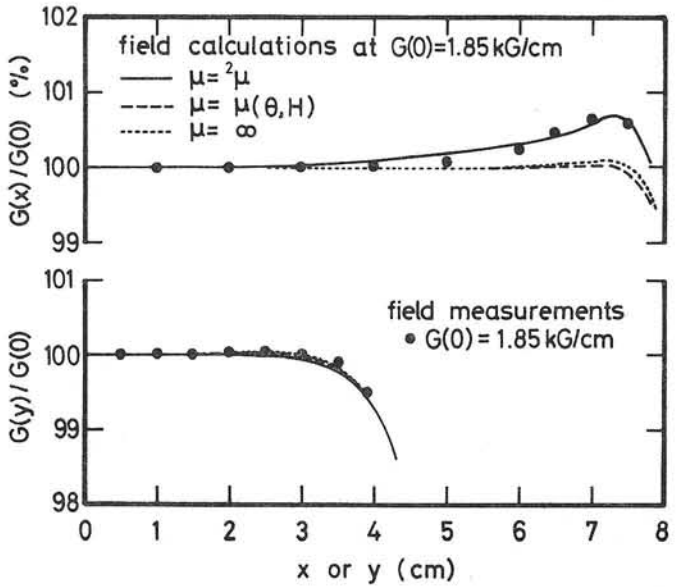

Fig.4 Distributions of field gradients on the horizontal (upper) and vertical (lower) median planes for the vertically oriented quadrupole magnet. Solid circles are the experimental data.

the computation. As the magnetic properties of the non-oriented magnet, was assumed the compiled $B^2 - \gamma$ table in the original program.

Generally, the magnetic flux lines are not parallel with the magnetizing force in the media with magnetic anisotropy. In computation, two curves of 0 and 90 deg. in Fig.1 were assumed for the transverse magnetic properties. But it is difficult to derive another curves from these ones at the present stage of the work even if the angular difference between B and H is taken into account. It is rather interesting that the second approach gives the good coincidence with the magnetic measurement.

Authors should like to express their thanks to Prof. T. Nishikawa for his continuous interest and invaluable discussions. They also acknowledge Messrs T. Igarashi and A. Araki for their efforts paid to the field measurements.

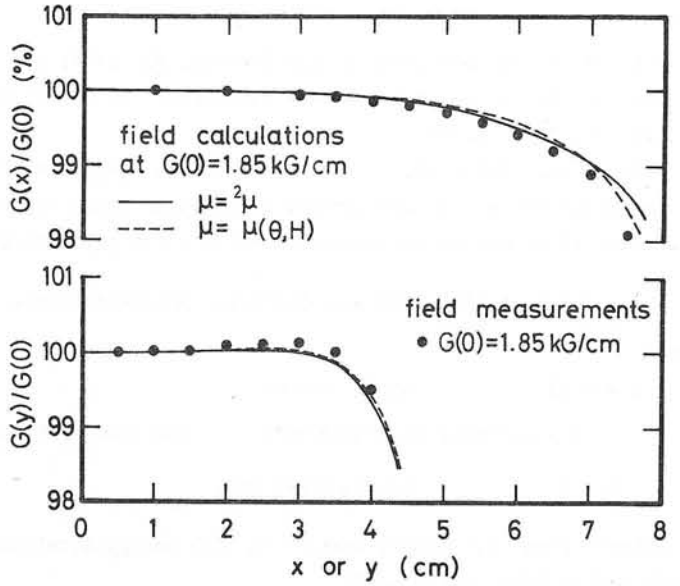

Fig.5 Same as in Fig.4 for the horizontally oriented quadrupole magnet.

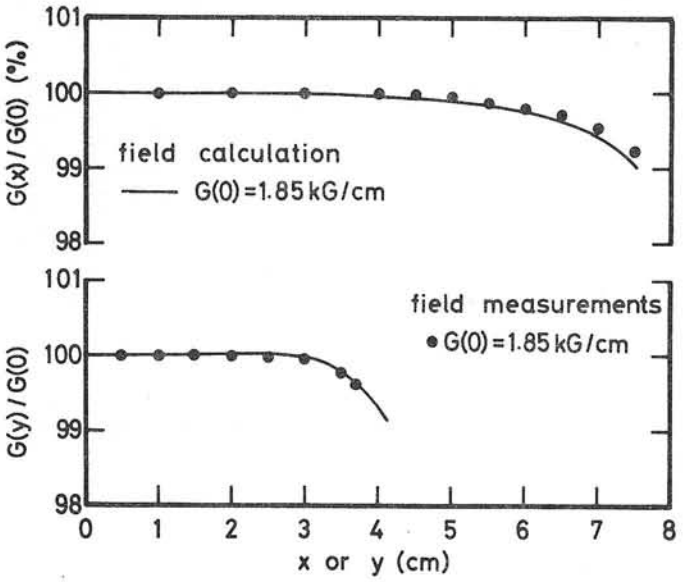

Fig.6 Same as in Fig.4 for the non-oriented quadrupole magnet.

References

1) T. Doke et al, Nuclear Instrum. and Methods, 83 (1970) 300

2) K. Endo and M. Kihara, Proc. of 4th Intl. Conf. on Magnet Technology, Brookhaven, 1972, p.306

3) K. Endo et al, IEEE Trans. on Nuclear Science, NS-20 (1973) 716

4) The experimental curves were provided by Nippon Steel Corporation.

5) Function $f(\theta,H)$ may be approximated within a few percents by

$$f = 0.025 \sin 6\theta + 1/\{0.4+2.35\alpha+(0.6-2.35\alpha)(\sin\theta+\cos\theta)\},$$

where

$$\alpha = 0.25 \quad , \qquad \text{for } H > 600 \text{ Oe}$$

$$= -5.3\times10^{-7}H^2+7.3\times10^{-4}H+2\times10^{-3} \quad , \qquad \text{for } 40 < H \leq 60 \text{ Oe}$$

$$= 0.0 \quad , \qquad \text{for } 0 \leq H \leq 40 \text{ Oe} .$$

6) M. Kihara, Proc. U.S.-Japan Seminar on High Energy Accelerator Science, Tokyo and Tsukuba, 1973, p.134

Fields Involved in Magnetic Recording on Moving Steel Strip

by E. M. Deeley and L. Hayali

Summary

A finite-difference method is described for solving field distributions relating to magnetic recording on steel strip, in which hysteresis, eddy-currents, and strip motion are taken into account. The method is sufficiently general to allow other nonlinear phenomena to be studied. A hysteresis model based on the arctan function is used which can be adjusted to approximate practical loops sufficiently closely.

An implicit time-stepping method is used together with nonlinear over-relaxation which gives convergence rates comparable with those for linear problems, even when the medium is heavily saturated. The inherent stability of the implicit method allows large time steps to be taken, particularly during the initial transient period.

An alternative method using equivalent currents to represent magnetization has also been used.

1. INTRODUCTION

The accurate measurement of the speed of moving steel strip by pulse or sinusoidal magnetization methods has led to the need for a better understanding of the recording process itself. Various studies of recording on non-conducting media have been made [1,2,3] but the process of recording onto steel does not appear to have been studied in detail. The representation of hysteresis is a necessary feature of the computation, but as remnant magnetization is fundamental to the process it is not possible to employ complex permeability and a more physical model of hysteresis must be used. In addition, eddy-currents and the motion of the recording medium must be taken into account.

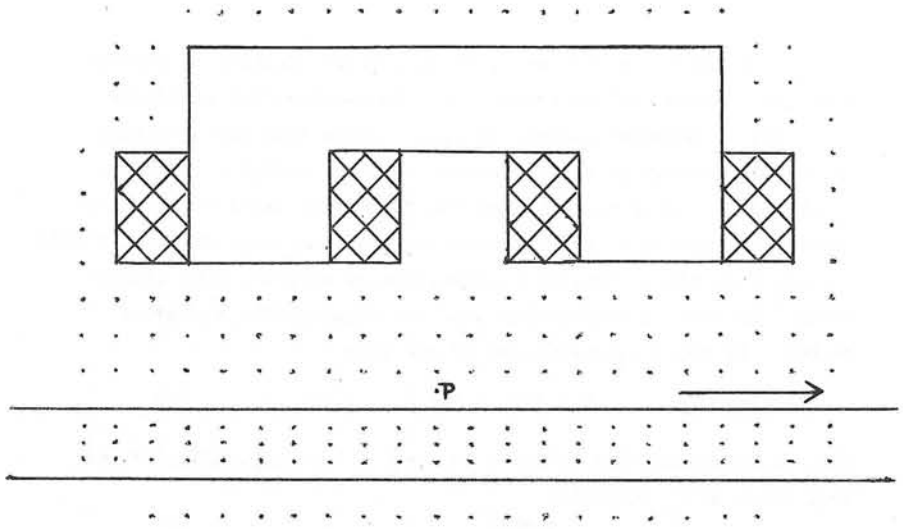

Fig. 1. Recording Head and Strip (current coils shown hatched)

The arrangement of the ferrite recording head, exciting coils, and steel strip is illustrated in fig. 1. A square mesh is used with a 3mm spacing, reducing to a rectangular mesh in the strip. This reduction ratio, and the node spacing in general, can be easily modified. In practice it is desired to study the effect of the separation between recording head and strip over a frequency range of approximately 4-250 Hz, and of strip speed.

The programme developed to simulate this process has also been used to study other nonlinear phenomena.

2. THE COMPUTATIONAL METHOD

Various finite-difference methods have been used to solve non-linear magnetic field problems, including alternating-direction and extended Liebmann methods. In the present work the parabolic diffusion equation :

$$u_{xx} = k_1 u_t + k_2 u_x \qquad (1)$$

is solved by an implicit time-stepping method. The simplest scheme

is that described by O'Brien [4], while greater accuracy is possible with the Crank-Nicholson scheme [5] at the expense (for nonlinear problems) of somewhat greater storage. These have the advantage that the equations solved are essentially the elliptic equations of the equivalent static problem, the additional terms due to time variation behaving as source terms, so that the computation is stable for any time step. Nonlinear relaxation as originated by Lieberstein [6] is used in conjunction with the Gauss-Seidel iterative method. If the N equations are of the form :

$$g_p(x_1, x_2, \ldots\ldots x_N) = 0 \quad p = 1,2, \ldots. N \qquad (2)$$

then an overrelaxation factor ω is used in the computation of the next value of x_p such that :

$$(x_p)_{n+1} = (x_p)_n - \omega\left(\frac{dx_p}{dg_p}\right)(g_p)_n \qquad (3)$$

where n refers to the n^{th} iteration. The derivative appearing in this equation is calculated node by node, making use of the most recently corrected results as in the linear SOR method. This calculation is straightforward if analytic expressions are used for the non-linearities present, and the rate of convergence is comparable with that for linear problems.

Writing the non-linear relationship between B and H as :

$$B = \mu_o f(H) \qquad (4)$$

then for the conventional five-point star in the x-y plane as shown in fig. 2, for which the node spacing, h, is the same for each connection, the z-component of Curl H becomes :

Fig. 2

$$(\text{Curl } H)_z = \frac{1}{\mu_o h}\left[f^{-1}(B_{03}) - f^{-1}(B_{20})\right] - \frac{1}{\mu_o h}\left[f^{-1}(B_{10}) - f^{-1}(B_{04})\right]$$

$$= \frac{1}{\mu_o h}\sum_{i=1}^{4} f^{-1}\left(\frac{A_o - A_i}{h}\right) \qquad (5)$$

which can be equated to J_z in accordance with Maxwell's equation. For moving media the vector current density is :

$$\overline{J} = \sigma(\overline{E} + \overline{v} \times \overline{B}) \qquad (6)$$

where $\overline{v}$ is the velocity vector. If the only component of $\overline{v}$ in the two-dimensional case is v_x, then (6) becomes :

$$J_z = -\sigma \frac{\delta A}{\delta t} - \sigma v_x \frac{\delta A}{\delta x} \qquad (7)$$

Using a backwards difference expression for $\delta A/\delta t$, and a central difference expression for $\delta A/\delta x$, averaged between the present and previous time steps, equation (7) becomes :

$$J_z = -\frac{\sigma}{\Delta t}\left[(A_o)_{k+1} - (A_o)_k\right] - \frac{\sigma v_x}{4h}\left[(A_3)_{k+1} + (A_3)_k - (A_1)_{k+1} - (A_1)_k\right] \qquad (8)$$

where k and k+1 refer to successive time steps and Δt is the length of the step. Combining this with equation (5) to form Curl H - J=0 gives

$$g_p(A_o) = 0 \qquad (9)$$

The values of $(A)_k$ in the conducting region, must therefore be stored, and this formulation is then essentially that of O'Brien et al. If values of Curl H at the k^{th} step are also stored and averaged with those calculated by equation (5), the Crank-Nicholson form is obtained. In this method independent values of H, and hence of incremental permeability, are attributed to each connection in the 5-point star.

Differentiating $g_p(A_o)$ with respect to A_o gives :

$$\frac{dg(A_o)}{dA_o} = \frac{1}{\mu_1} + \frac{1}{\mu_2} + \frac{1}{\mu_3} + \frac{1}{\mu_4} + \frac{\sigma\mu_o h^2}{\Delta t} \qquad (10)$$

where $\mu_1 \ldots. \mu_4$ are the slopes df/dH of the nonlinear B-H functions at the four operating points, and is the factor required for the nonlinear over-relaxation of equation (3).

Modified forms of equations (5) can be found for nodes on the boundary of the non-linear medium, or where a change of mesh size takes place, or where both occur together. In computing vector potential it is convenient to allow the numerical values to represent A/h at each node, as this quotient appears in the non-linear functions. This representation is therefore also used in the remainder of the field, the exciting current appearing in the form I/h, where I is the actual current concentrated at a node.

An Equivalent Current Method

By using for Curl H the expression :

$$\text{Curl } H = \frac{1}{\mu_o} \text{ Curl } B - \text{Curl } M$$

and representing Curl M by an equivalent current, J_e, there results :

$$\text{Curl } B = \mu_o (J + J_e)$$

or in vector potential terms :

$$\nabla^2 A = - \sigma\mu_o \frac{\delta A}{\delta t} - \sigma\mu_o v_x \frac{\delta A}{\delta x} + \mu_o J_e \qquad (11)$$

In this approach, which has been used in an integral method by Robertson and Zaky [7], the nonlinear properties of the medium are contained in J_e. In the finite difference version of this method the equivalent currents are calculated after each complete sweep of the field used to calculate the values of A, so that acceleration of both A and J_e can be used. If a node-by-node computation of J_e is used the method reduces to a Curl H formulation similar to that already described.

The equivalent current method has proved successful for thin structures of not more than two node spacings in depth, where with appropriate choice of both acceleration factors it converges rapidly. For thicker regions however, the method traps residuals so that the convergence rate is slow.

3. THE HYSTERESIS MODEL

Several hysteresis loop models of varying degrees of complexity have been proposed to represent metallic and non-metallic magnetic materials. These include piecewise-linear [2,8], simple algebraic and trigonometrical functions used in conjunction with variable control parameters [1,9,10], and more complex models using two or more non-linear functions [11]. A necessary feature of any model is the ability to represent minor loops, and in the simulation of a hysteresis motor Jackson [8] has used a piecewise-linear model with five control parameters which operates in any of nine different modes. Sawamura and Iwasaki have also used such a model in studying tape recording processes [2]. Simple algebraic expressions may not fit practical loops particularly closely but have the advantage of simplicity and speed when the hysteresis routine is to be accessed many times. The model described by Everatt based on the Fröhlich equation [9] is probably the most suitable. Certain simple functions fit practical loops more closely [1, 12] at the expense of greater computing time, particularly if the inverse of the function is required. This is usually a problem if H is to be computed from B. Chua and Bass have described a very comprehensive model [11] making use of several functions which also represents dynamic effects, but would be prohibitively time-consuming in an iterative process.

In the present work the arctan function is used, shifted in position along the H-axis when the flux change is reversed in order to follow the major and minor loops [1]. This is used to represent magnetization, to which $\mu_o H$ is added to obtain flux density. The model can be adjusted to provide a close fit to actual static loops, such as those obtained for a steel sample by Zakrzewski and Pietras [13].

4. TRANSPORT EFFECTS

The magnetization of the strip is transported at the strip velocity and this effect must be represented at each time step. This is particularly easily arranged when the velocity is one node per time step, interpolation being necessary for other speeds.

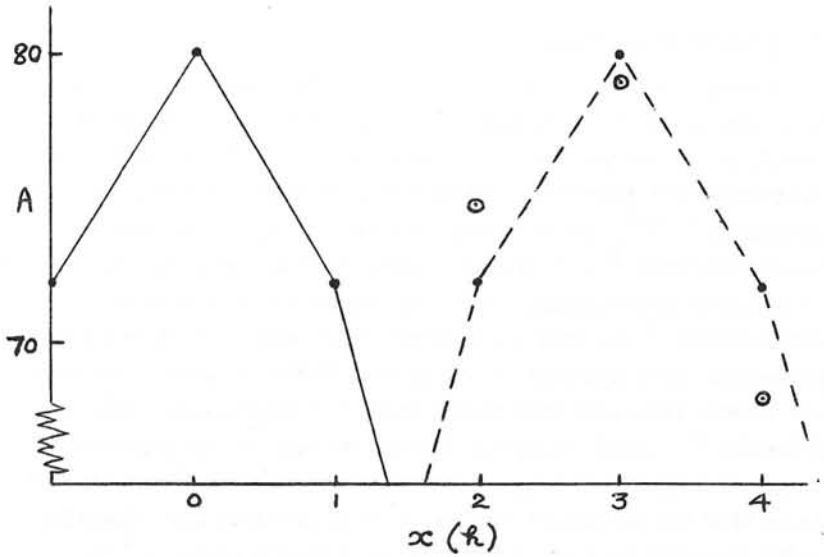

Fig. 3 Original distribution - solid line
Ideal distribution - broken line
Actual nodal values - circles

In the equivalent current method the J_e values represent the magnetization. Another transport effect is represented by the terms containing σ, and for an idealized situation when σ becomes infinite equation (9) reduces to :

$$-\frac{\partial A}{\partial t} = v_x \frac{\partial A}{\partial x} \qquad (11)$$

In these circumstances the vector potential pattern should be transported in the x-direction with velocity v_x, unchanged in form. The accuracy with which this transport effect is simulated depends on the truncation errors introduced by the finite-difference approximation to equation (11) and has been studied using a one-dimensional model. Figure 3 shows how the peak of a gaussian-shaped potential distribution starting a node 0 is modified after being transported over a distance 3h in 15 time steps. The solid curve indicates the initial distribution with the actual values at nodes indicated by circles, while the broken line shows the ideal distribution 15 time steps later. The backward time difference and central space difference averaged between time steps used in equation (8) leads to actual potential values illustrated by circles in Figure 3. An attenuation of the distribution by about ½% at its peak is observed, while there is a lagging effect in the velocity of the distribution of approximately 10% below the expected velocity. When a higher order approximation to $\partial A/\partial x$ is used however, so that the truncation error is reduced to $O(h^3)$, the error in the velocity is reduced to less than 1%.

Experiments with higher order approximations to both derivatives indicate that the amplitude error is reduced by reducing the truncation error in $\partial A/\partial t$, while the velocity error responds to improved expressions for $\partial A/\partial x$. Various methods have been devised for reducing errors in the computation of equation (11), which have been summarized by Ames[14] and further reduction of the above errors is possible, although not necessary in the present study where the major transport effect is by remnant magnetization.

A further effect caused by the moving medium is the build-up of spurious vector potential values at points of entry to, and exit from, the computed field. This is particularly severe if a boundary condition of A=0 is imposed, but can be reduced by employing a derivative boundary condition.

The use of a hysteresis loop necessitates storing values of B and H at each iteration in order to define the point reached on the loop. These values must be moved with the strip at each time step, but the presence of the $\partial A/\partial x$ term in equations (7) and (11) removes the need to move values of A. If the values of A stored at the end of a time step are also moved with the strip, however, the $\partial A/\partial x$ term can be deleted.

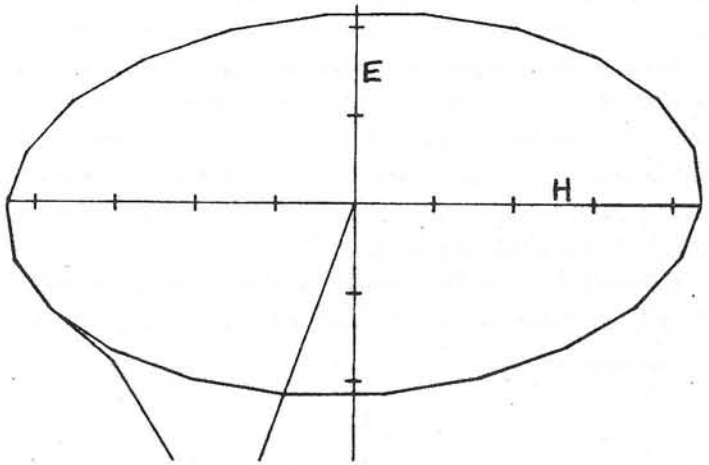

Fig. 4 - E/H Relation using O'Brien method

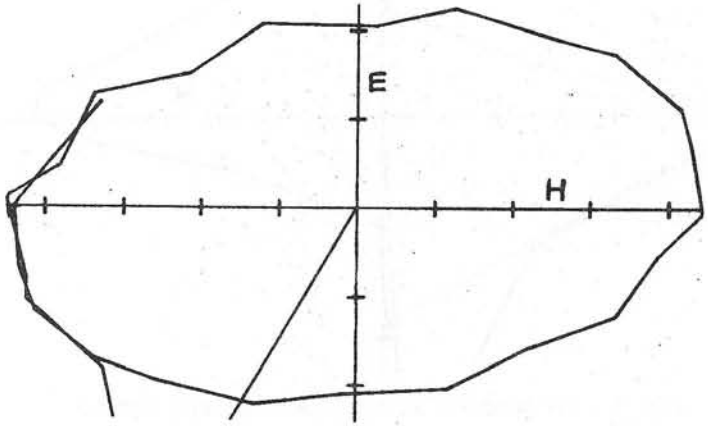

Fig. 5 - E/H Relation using Crank-Nicholson method

5. RESULTS

For comparison purposes various studies have been carried out using linear material for the strip, as well as non-linear material without hysteresis. The equivalent current method has also been used for moving material with hysteresis.

(a) Studies with Linear Material

Results for linear material were obtained using the model shown in figure 1, with the same mesh spacing throughout the region. The frequency used was such that the strip thickness equalled twice the penetration depth at a relative permeability of 1000, and 22 time steps per cycle were employed.

In order to study the behaviour of different computational schemes, the relationship between tangential electric and magnetic fields was observed at a distance h/2 above the top surface of the strip, at a point between the poles (marked by P in figure 1). Simple finite difference expressions using the nodes above and below P, and those stored for the previous time step, were used. This relation is illustrated in figure 4 using the method of O'Brien et al, from which it is seen that after an initial transient the computation rapidly settles to its steady-state condition. The apparent phase angle between E and H is more nearly equal to 90° than 45°, this being due to the mesh representation of the region. (A very much finer mesh in the strip region would improve this situation, which in network terms would cause the strip to appear more as a transmission line than as a capacitance as seen from the air region).

A similar result is illustrated in figure 5 for the Crank-Nicholson method which, while employing more exact finite difference expressions with smaller truncation errors, is seen to follow a zig-zag oscillatory path before reaching its steady-state response after about one cycle. This numerical oscillation is considerably worse in parts of the field where only small differences are taken to calculate E and H, and appears mainly in the calculation of H. Inadequate convergence at each time step, which is not easily detectable in the O'Brien method, very much increases the amplitude of numerical oscillations in the Crank-Nicholson method.

Consideration of the corresponding network model of the field distribution indicates how a more accurate relation between tangential E and H can be found by also making use of values of vector potential at neighbouring nodes on the surface of the strip. By this means a phase angle of 42° is measured on the surface below point P, which is close to that expected. Where the component of

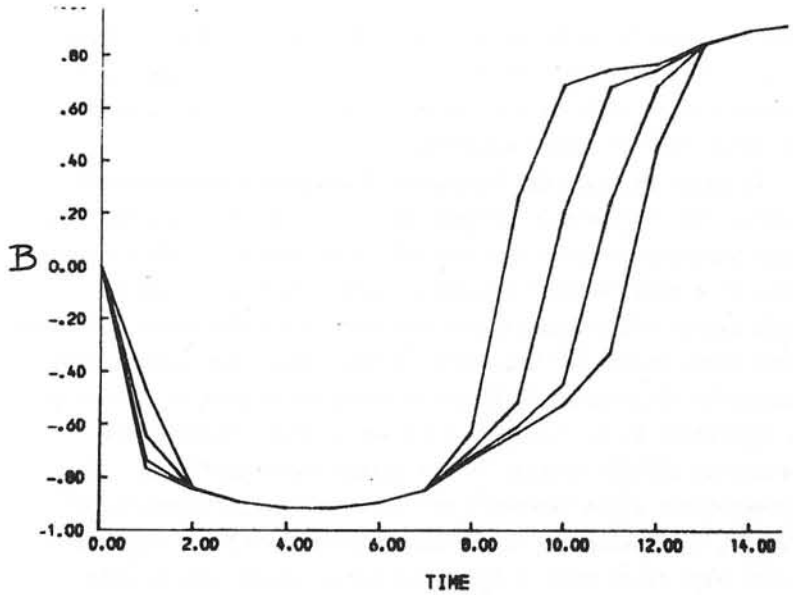

Fig. 6 - A wave of flux change in nonlinear material

normal flux is large, such as below the poles, further errors are introduced into the calculation of the tangential fields, the measured phase angle at these particular points being 57°.

(b) Non-linear material

For studies with non-linear material the B-H curve was represented by the particular Frölich equation:

$$B = \frac{H}{300 + 1.25|H|} + \mu_o H$$

where B is Teslas and H in A/m. This gives an initial permeability of about 1000 and a saturation magnetization of 0.8T. Using an exciting current which would have produced a maximum flux density of approximately 2.5T in linear material having the same initial permeability the non-linear over-relaxation procedure worked well, the rate of convergence being approximately 0.6 that for the linear problem. The optimum acceleration factors were 1.88 (linear) and 1.85 (non-linear) respectively. Experiments with very deep saturation using a current drive ten times greater still necessitated a reduction in acceleration factor to 1.65, the convergence rate being approximately 0.3 times that for the linear problem.

For the lesser degree of saturation fig. 6 illustrates the flux density at four levels in the strip for the first half cycle of excitation using the O'Brien method. These levels are those directly beneath P (fig. 1) and illustrate the characteristic rapid change in flux between the saturation levels at progressively later times as the material is penetrated[15].

Similar behaviour is observed under each pole, and greater excitation produces faster switching and more rapid progress of the wave, as expected.

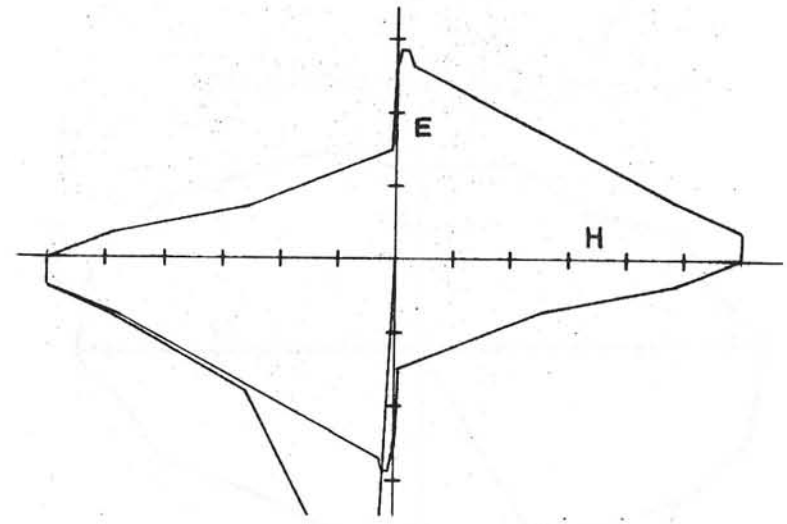

Fig. 7 - E/H Relation on Non-linear Material Surface

The relation between tangential E and H on the surface below Point P is illustrated in fig. 7, although no attempt has been made to measure the phase angle between the fundamental components. This might be expected to lie between 26.6° and 45°.

(c) Hysterectic Material

The arctan hysteresis loop model has so far been used only in conjunction with the equivalent current method. Preliminary results

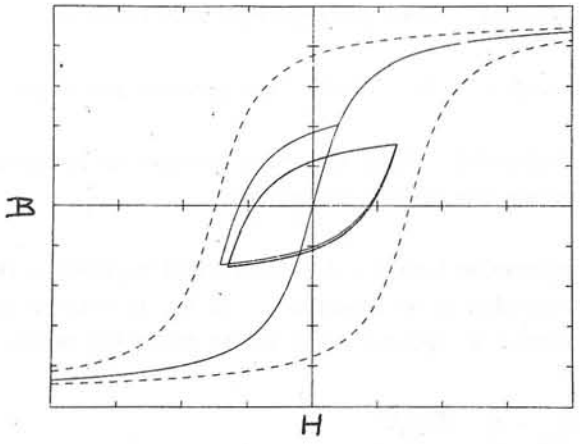

Fig. 8 - Transient and Minor loop in stationary strip

for a simple model employing a single coil recording head and strip of thickness equal to 2h have been obtained for various frequencies, for both stationary and moving strip. For a frequency at which the thickness is approximately one-half of the penetration depth for the initial permeability used, figure 8 illustrates the form of the magnetization loop reached after an initial transient, at a point on the surface of stationary material in the vicinity of the exciting coil.. It has also been found practicable to examine the variation of magnetization in moving strip at a point remote from the exciting coil, which is the essential requirement for studying magnetic recording phenomena. No detailed studies of this have yet been made, however.

CONCLUSIONS

Implicit time-stepping methods have been used on linear, non-linear, and hysteretic material with the object of studying the magnetic recording produced on moving steel strip by a writing head. An equivalent current representation of magnetization has been used in conjunction with an arctan hysteresis model to obtain preliminary results using both stationary and moving strip, but the poor convergence rate of this method when the strip is greater than two nodes in thickness preclude its use for more detailed studies. This disadvantage is found to be due to the trapping of residuals within the magnetic material when the equivalent currents are computed alternately with vector potential on a field-by-field basis.

The use of a formulation based on Curl H together with non-linear over-relaxation is found to give excellent convergence using either the O'Brien et al or Crank-Nicholson implicit schemes, although the latter is found to go through a number of numerical oscillations before reaching a steady state. There appears to be no difficulty in principle in extending this approach to moving hysteretic material, which represents the next stage of the present work.

7. ACKNOWLEDGEMENTS

The authors would like to thank Mr. J. Carpenter of Imperial College for many useful discussions.

8. REFERENCES

1. George, D.J., King, S.F., and Carr, A.E. "A self-consistent calculation of the magnetic transition recorded on a thin film disk". I.E.E.E. Trans. MAG-6 pp.240-3 (1970).
2. Sawamura, S., and Iwaraki, S-I. "Application of the internal reaction field on the Analysis of Anhysteretic Magnetizing Process". I.E.E. Trans. MAG-6 pp.646-49 (1970).
3. McCary, R.O. "Saturation Magnetic Recording Process" I.E.E.E. Trans. MAG-7 pp.4-16, (1971).
4. O'Brien, G.G., Hyman, M.A., and Kaplan, S. "A Study of the Numerical Solutions of Partial Differential Equations." J. Math. Phys. 29 p.223 (1950)
5. Crank, J. and Nicholson, P. "A Practical Method for numerical evaluation of solutions of partial D.E.^{S} of the heat conduction type". Proc. Camb. Phil. Soc. 43 pp.50-67(1947)
6. Lieberstein, H.M. "Over-relaxation for non-linear elliptic partial differential equations". Tech-Rept. No. MRC-TR-80. University of Wisconsin Mathematical Research Centre (1959).
7. Zaky, S.G. and Robertson, S.D.T. "Integral Equation formulation for the solution of magnetic field problems" (Part I). Trans. I.E.E.E. PAS-92 pp.808-815 (1973).

8. Jackson, R.D. "Digital Simulation of the hysteresis motor" Proc. I.E.E. 120 p.1533-7 (1973).
9. Everatt, J.S. "Computer Simulation of non-linear inductors with hysteresis". Electron. Lett.6 pp.833-4 (1970).
10. Curland, N. and Speliotis D.E. "A theoretical study of an isolated transition using an iterative hysteretic model". I.E.E.E. Trans. MAG-6 pp.640-46 (1970).
11. Chua, L.O. and Bass, S.C. "A generalized hysteresis model" I.E.E. Trans. CT-19 pp.36-48 (1972).
12. Stoll, R.L. "The Analysis of Eddy Currents". (Clarendon Press, Oxford) p.90 (1974).
13. Zakrzewski, K. and Pietras, F. "Method of calculating the electromagnetic field and power losses in ferromagnetic material, taking into account magnetic hysteresis". Proc. I.E.E.118 pp.1679-85 (1971)
14. Ames, W.F. "Numerical Methods for Partial Differential Equations". (Nelson) pp.232-38 (1969).
15. Agarwal, P.D. "Eddy Current losses in solid and laminated iron". Trans- Amer. Inst. Elect. Engrs. 78 (Pt.II) pp.169-8 (1959)

Discussions following paper:

(Reichert, Brown Boveri) Have you neglected Eddy Currents?

(Deeley, Kings College) No. $\partial A/\partial t$ term accounts for these.

(Polak, Philips Eindhoven) Which equations are used at the material interfaces to complete the problem definition.

(Deeley) The expression Curl H = J is sufficient to specify the vector potential equation at an interface. If H_{o1} is written in terms of the vector potential at nodes 0 and 1 in the following manner (for linear material):

$$H_{o1} + \frac{1}{\mu} B_{o1} = \frac{1}{\mu} \frac{Ao - A1}{h}$$

and similar expressions written for the other connections to node 0, then substitution into Curl H=J yields the familiar expressions for vector potential relations at interfaces and corners.

MATHEMATICAL MODELLING OF MAGNETIC HYSTERESIS

by N. JANSSENS
Faculty of Applied Sciences
University of Louvain

Abstract

The aim of this study is to build, for polycristalline ferromagnetic bodies, a general model of hysteresis to be used as a framework for comparing the various mathematical models which have been proposed.

One only relies upon the properties of the experimental magnetization curves since the value of a given model is ultimately measured by the accuracy with which experimental curves can be predicted.

This approach makes it possible to prove on purely phenomenological grounds, without any recourse to microscopic physics, the validity of a generalized Preisach model.

This leads to a model of hysteresis which is fully justified and relatively easy to handle. Furthermore, it shows which experimental characteristics are the most relevant for the calculation of the "Preisach density".

1. Magnetization curves

In order to build models of the magnetic hysteresis phenomenon, we will begin with a detailed analysis of experimental magnetization curves and point out their fundamental characteristic features.

1.1. A property of almost every magnetic material is symmetry with respect to the origin (H=0, M=0) of the magnetization curves for evolutions of opposite signs.

Although this simplifies the models, the following developments do not refer to this property so that we will, for instance, be able to represent the asymmetric cycle of a permanent magnet cooled in a magnetic field.

The symmetry property will thus provide us with an additional relation within every model.

1.2. Another fundamental characteristic can be idealized by stating that :

> Secondary cycles are closed and, after being closed, have no more influence on the subsequent evolution (we will say they are forgotten).

Figure 1 shows how accurately this statement is verified for a given material (ARMCO 0202). A model having such a property eliminates the accomodation phenomena (stabilization and drift of successive cycles).

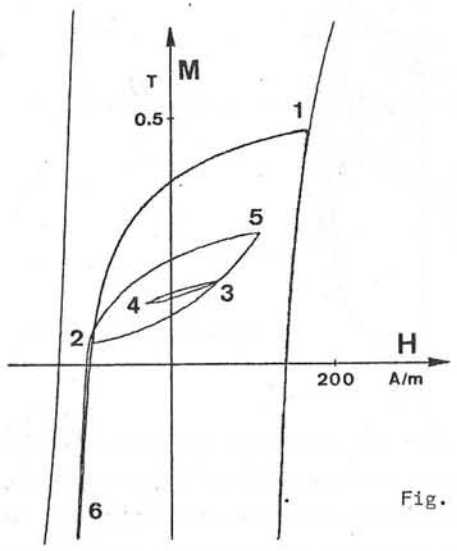

Fig. 1 Secondary cycles

Some hitherto proposed representations of magnetic hysteresis do not comply with this requirement. For instance, the model proposed by Duhem [1] aims to describe the magnetic state of a material with the only two variables H and M by considering two curves passing through each point inside the limit cycle, one to be used for increasing, the other for decreasing field and magnetization. Other models [2, 3, 4] are similar to the preceding one or particular cases of it. Their utility seems limited since, for some kinds of evolutions, their predictions are far from approximating the real behaviour of the material. This is shown on figure 2 by evolution 1 2 3 4 5 which is based on a model of this type and deviates appreciably

from any experimental curve.

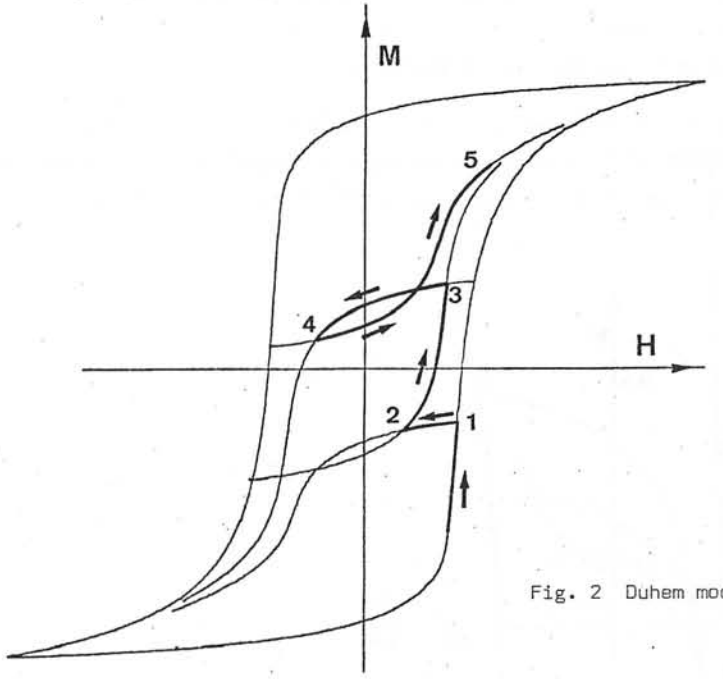

Fig. 2 Duhem model

Such models may only be used when the monotonous parts of an evolution are of great amplitude, compared with the width of the limit cycle. In this case, indeed, the magnetization curves are so close to the limit cycle that the closing and forgetting of the secondary cycles becomes of little importance.

Let us notice that the model we will establish (par.2) makes it possible to give a very simple (although rather crude) description of hysteresis with H and M uniquely determining the magnetic state and where the secondary cycles are closed and forgotten. This is shown on figure 3 : the evolutions are reversible inside the limit cycle and irreversible on this cycle.

1.3. A statement which is satisfied with the same accuracy as the closing and forgetting of the secondary cycles is the following :

> Inside a secondary cycle, the magnetization curves depend only on their starting point.

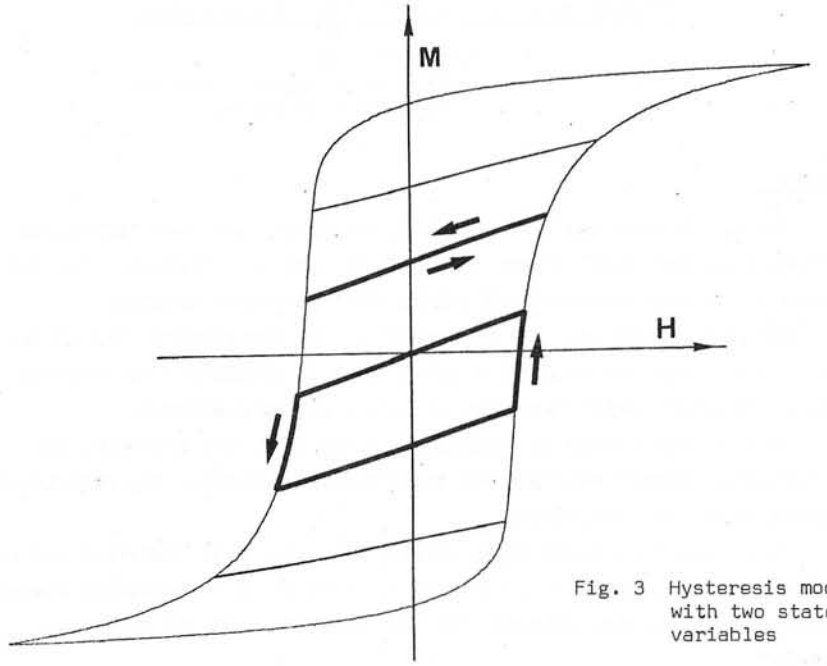

Fig. 3 Hysteresis model with two state variables

Figure 4, for instance, shows that the evolutions 1 2 3 2 4 and 1' 3 1' practically coïncide upon the path 3 2 . There is a certain analogy between this property and the ideas which form the basis of Duhem's model. In both cases, indeed, the curves depend only on the starting point in a given direction. However, here, the utilization of the curves to be followed is so restricted that the physionomy of the model is entirely different.

1.4. The preceding idealization requires the knowledge of a double infinity of curves. It may be seen that an important simplification is introduced at the expense of a small reduction in accuracy if one states that :

> The curves issued from points located on each of the straight lines of fixed slope - 1/k are deduced from each other by translation

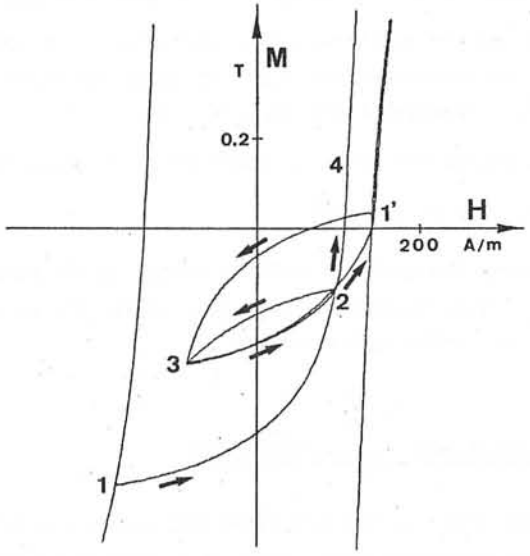

Fig. 4

Evolutions inside secondary cycles

If (H_e, M_e) is a point of the descending (ascending) limit cycle, the equation of the ascending (descending) curve starting from (H_i, M_i) located on the straight line with slope -1/k passing through H_e, M_e has thus the form :

$$M - M_i = f(H-H_i, H_e+kM_e) \qquad (1)$$

(The use of $H_e + kM_e$ as a parameter instead of H_e or M_e will prove to be convenient at a later stage).

Figure 5 shows that the last statement is in good agreement with experiment. The value of the parameter k is choosed from the magnetization curves in such a manner that one gets the best possible verification.

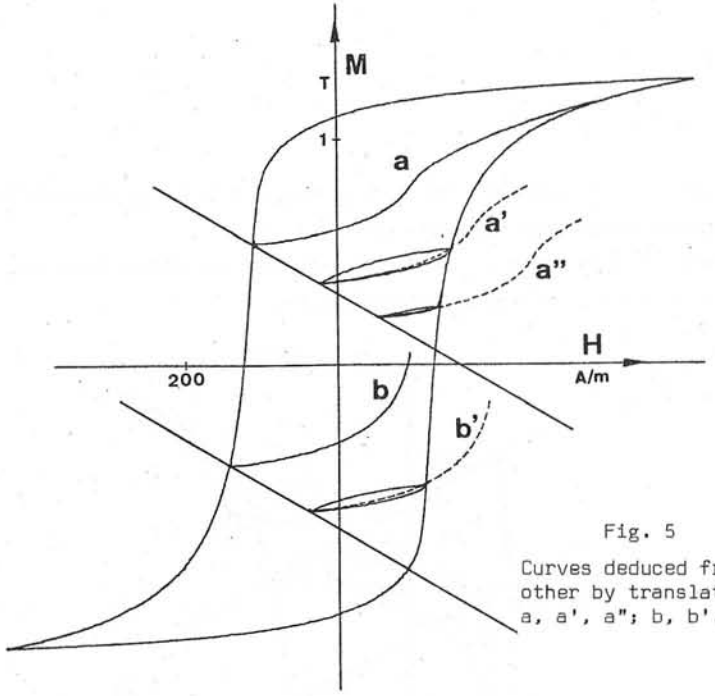

Fig. 5

Curves deduced from each other by translation : a, a', a"; b, b'.

2. Proposed Model.

The above statements leads us to the following model.

We consider the family of experimental ascending and descending curves starting from each point (H_e, M_e) of the left respectively right side of the limit cycle. Their equations are given by (1) for $(H_i, M_i)=(H_e, M_e)$ and by introducing for every pair of (H,M) the new variable

$$H' = H + kM$$

they can be transformed into

$$M - M_e = g(H', H'_e) \qquad (2)$$

According to statement 1.4, the ascending evolution starting, after reversal of the direction, from point (H_A, M_A) located on the straight line with slope -1/k passing through (H_e, M_e), has to be given by

$$M - M_A = g(H', H'_e)$$

or, since $H'_A = H'_e$,

$$M - M_A = g(H', H'_A) \qquad (3)$$

The construction is shown on figure 6 as wel as the curve corresponding to the following reversal at point B.
As indicated on the figure, the use of experimental curves does not in general give exactly closed secondary cycles.

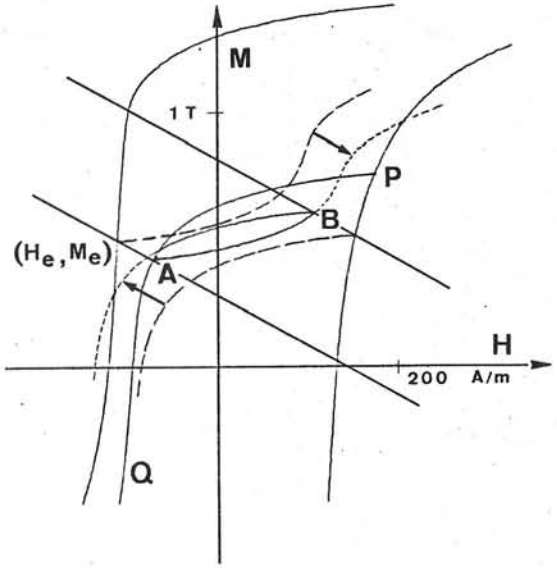

Fig. 6 "Construction" of the magnetization curves

In order to satisfy statement 1.2, the curves (3) must obey the relation

$$M_B - M_A = g(H'_B, H'_A) = - g(H'_A, H'_B)$$

To obtain this result we modify the experimental curves (2) and use for the model the expression

$$M-M_e = g_c(H',H'_e) = \frac{1}{2} [\, g(H',H'_e) - g(H'_e, H') \,]$$

This change affects the curves only slightly (in fact to the extent the previous statements are not fully verified experimentally).

To complete the model, we only have to add that, after coming back to point A, the subsequent evolution is the continuation of curve P A followed before reaching A for the first time.

If applicable, the symmetry statement (1.1) takes the form

$$g(H'_B, H'_A) = - g(-H'_B, -H'_A)$$

In summary, the proposed model is formed by the family of almost experimental curves issued from the limit cycle, the parameter k and a simple rule for combining the curves.

3. Identification with the Preisach model

3.1. One knows that the Preisach model represents a polycristalline ferromagnetic material by an assembly of dipoles having rectangular hysteresis loops displaced a distance h_f away from the origin and with a coercive force h_c (figure 7). The fluctuation field h_f takes into account the interaction of the neighbouring dipoles [5,6] . The density $\varphi(h_c, h_f)$ of the dipoles characterized by h_c and h_f can be represented in a plane where a line formed by segments alternatively at 45° and - 45° provides the state of the system (figure 8).

In order to get a good agreement with experiment, this model has to be expanded in two ways. Firstly, we take the reversible permeability into account [7,8] by adding on the axis $h_c=0$ a line distribution of dipoles $\phi(h_f)\delta(h_c)$. Secondly, as indicated in [10] and used in [9] , we replace the variable H by $H' = H + k'M$. This introduces a mean interaction field proportionnal to M.

The differential expression of a magnetization curve has then the form (figure 9) :

PERMANENT MAGNET MODELLING FOR MACHINE APPLICATIONS

W. Lord

Hoover Electrical Machines Group
Department of Electrical and Electronic Engineering
University College, Cardiff

ABSTRACT

Permanent magnet materials are used widely in the construction of all types of electrical machinery, from fractional horsepower stepping motors for incremental motion control to dc machines of 100 horsepower for rolling mill applications. With the increasing availability of high energy ferrite, alnico and rare earth magnets, it is imperative that design techniques for magnetic structures containing permanent magnets be improved to yield optimum utilization of the permanent magnet materials.

This paper reviews the application of permanent magnet materials to electrical machinery, particularly with regard to the complex recoil behaviour which exists in dc machines, alternators and stepper motors under dynamic operating conditions. Suggestions are made for adapting finite element algorithms to include the effects of complex recoil phenomena caused by the heavy demagnetization forces experienced in practice and other problem areas relevant to permanent magnet design are identified for further consideration.

INTRODUCTION

Future advances in permanent magnet technology as applied to electrical machine design will come, not only from the development of new materials, but also from improved design techniques. With the increasing availability of high energy ferrites, columnar crystal alnicos and rare earth magnets, it is imperative that advantage be taken of modern numerical analysis techniques in the design of permanent magnet (p.m.) poles for electrical machines in order to minimize the volume of magnet required. Current 'trial-and-error' approaches to p.m. design, although contributing to the 'black-art' aura surrounding the subject, do very little in terms of providing a sound basis on which to build the flexible, iterative design strategy needed for economical utilization of modern p.m. materials.

Considerable work still has to be done before the finite element and difference techniques, which have been so successfully applied to transformer and alternator design studies,[1-7] can be applied with equal success to permanent magnet structures. This paper discusses some of the factors affecting the use of numerical analysis techniques for p.m. design, including demagnetization forces in electrical machines and recoil loop modelling. Suggestions are made for incorporating these factors into finite element algorithms.

CURRENT DESIGN PRACTICE

Major aspects of permanent magnet design as applied to electrical machinery are summarized in Figure 1, with a typical p.m. motor construction shown in Figure 2.[8] It is normally assumed that

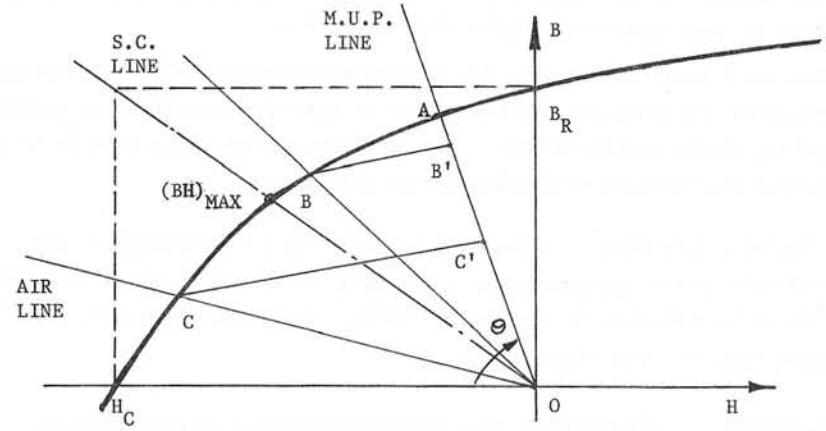

FIGURE 1 Permanent magnet design factors

all poles are initially in an unmagnetised state characterized by Point O at the origin of the B-H coordinates. Subsequent magnetization is assumed to take all poles into saturation, with a uniform flux density distribution resulting throughout the p.m. material. After magnetization it is assumed that all points on the surface of the pole work at point A, the intersection of the maximum unit permeance line with the major loop in the second quadrant.

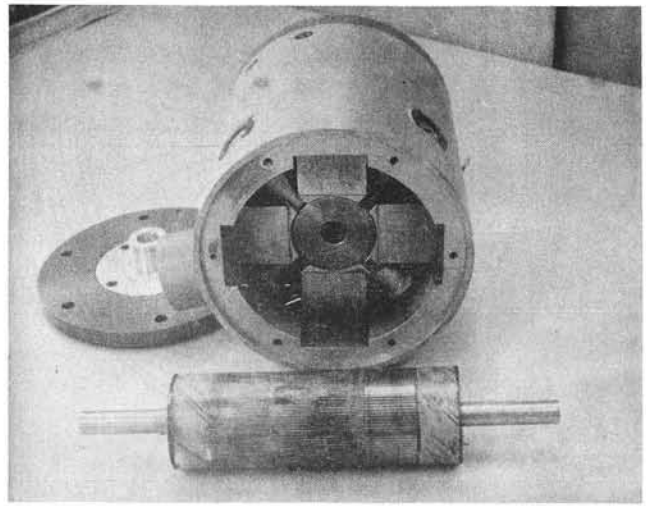

FIGURE 2 Permanent magnet motor construction

The angle θ can be used to define the maximum unit permeance line:

$$\tan \theta = \mu_o A_g L_m / A_m L_g \qquad (1)$$

Leakage and iron m.m.f. are often taken into account by using appropriate constants in equation 1. Stabilization of the magnet poles is then achieved by subjecting them to a demagnetization force greater than any likely to be experienced during operation. Short circuit and air stabilization lines are shown in Figure 1; demagnetization forces after stabilization, such as armature reaction m.m.f's, cause the magnets to work along lines BB' or CC'.[9] Ideally, for minimum magnet volume, the p.m. poles should be stabilized to operate close to the $(BH)_{max}$ point.

$$\text{Minimum P.M. Volume} = B_g^2 L_g A_g / \mu_o (BH)_{max.} \qquad (2)$$

Assumptions and approximations in this treatment are related to:

a) flux density distribution in the p.m. poles after magnetization
b) estimates of leakage factor and iron m.m.f.
c) recoil loop representation by a line
d) recoil line slope
e) demagnetization effects in electrical machinery.

All of these factors require further study in order to optimize the use of p.m. materials for machine excitation. Demagnetization forces are discussed in the following section as an illustration of how the physical phenomena associated with permanent magnet poles would affect numerical analysis techniques.

DEMAGNETIZATION PHENOMENA

Zakharov[10] first reported the excessive demagnetization effects in dc machines during reversal, and their effect on the flux density distribution under p.m. poles. This work has been substantiated by the author [11, 12] and Figure 3 shows the effects of reversal on the second quadrant operation of permanent magnet poles in a dc motor.

After short circuit stabilization all points on the surface of the p.m. poles would recoil to B', the flux distribution in a smooth rotor machine being similar to that shown in Figure 4.[13] On reversal, currents approaching twice the short circuit value are present in the armature giving a resultant flux distribution similar to that shown in Figure 5; one pole tip becomes heavily magnetized (point C in Figure 3) and the other heavily demagnetized (point D in Figure 3). After several reversals a non uniform flux density distribution exists over the magnet pole face, the centre of the pole working along recoil line BB', the pole tips working along DE. Attempts have been made to derive empirical relationships describing these effects,[14-16] but the results are not generally applicable to p.m. design.

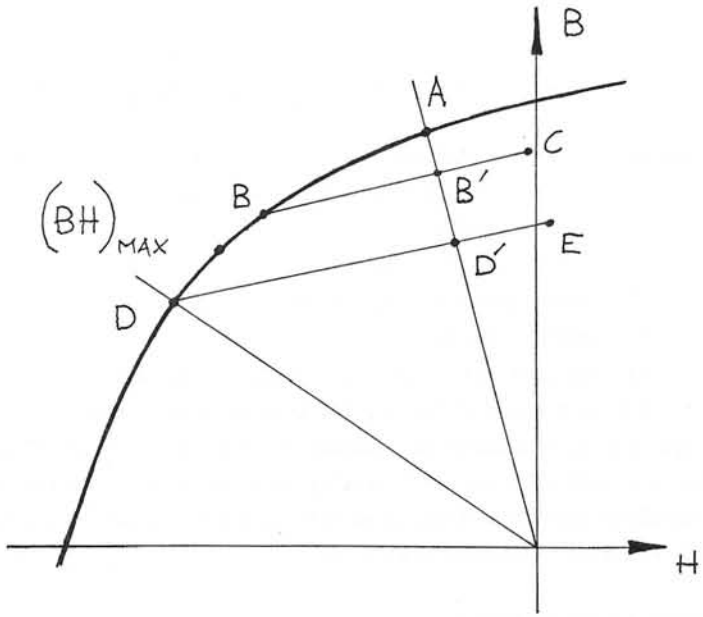

FIGURE 3 Demagnetization Phenomena in a Permanent Magnet DC Motor

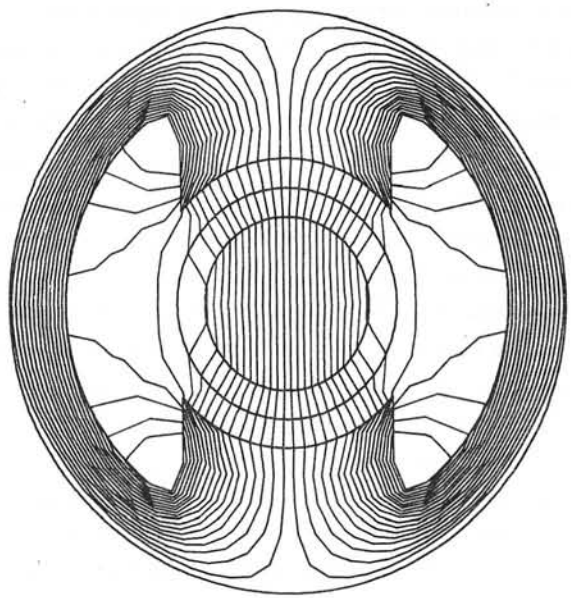

FIGURE 4 Flux distribution in an unloaded dc motor

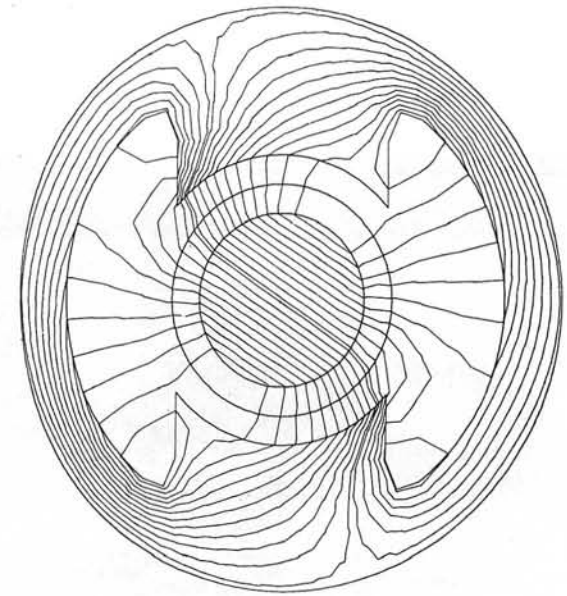

FIGURE 5 Flux distribution in a dc motor with heavy armature reaction

Similar effects are present during 'pull-in' and 'pull-out' modes of operation of p.m. stepper motors and synchronous machines. Figure 6 shows a simulated flux distribution in one quadrant of a four phase reluctance stepper motor,[13] and it is clear that the recoil behaviour of p.m. material on the rotor would be rather complex over the surface of the poles.

It is quite possible that with each part of a p.m. pole working along a separate recoil line, a 'minimum volume' design would entail the positioning of a band of recoil lines around the $(BH)_{max.}$ point, as shown in Figure 3 for the dc motor case.

The problem of optimum design becomes even more complex when rotor and/or stator slots are present and when it is realized that recoil line slopes can change by as much as 25% depending upon the point of origin on the major loop.[17]

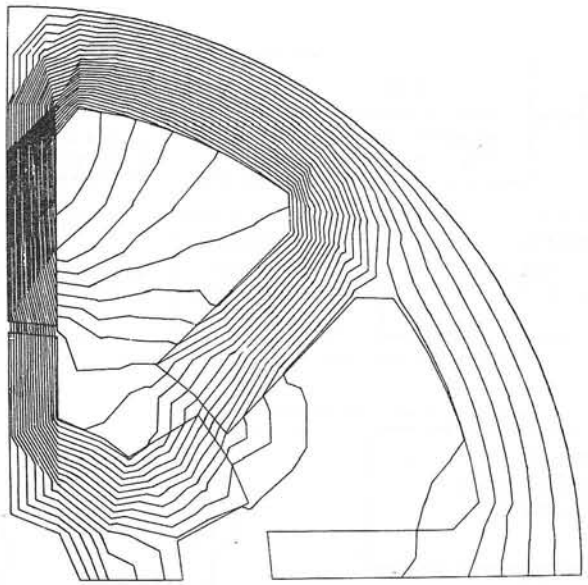

FIGURE 6 Flux distribution in one quadrant of a fourphase stepper motor

FACTORS AFFECTING NUMERICAL ANALYSIS OF P.M. STRUCTURES

Analysis of magnetic circuits in electrical machinery is based upon finding solutions of the nonlinear, poissonian-type equation

$$\frac{\partial}{\partial x}\left(\upsilon\frac{\partial A}{\partial x}\right) + \frac{\partial}{\partial y}\left(\upsilon\frac{\partial A}{\partial y}\right) = -J \qquad (3)$$

where A is the magnetic vector potential, υ is the reluctivity found from the nonlinear H/B characteristic in the case of the magnetic portions of the region being analysed, and J is the current density associated with the conducting portions of the circuit.

In finite difference methods[1,3] of analysis the partial derivatives of equation 3 are modelled over a rectangular mesh to yield a set of nonlinear algebraic equations of the form:

$$[SK]\,[U] = [F] \qquad (4)$$

where $[SK]$ is a square matrix containing nonlinear reluctivity terms, $[U]$ is a column matrix of nodal vector potentials and $[F]$ is a column matrix of current density terms.

A similar equation results from a finite element approach,[2,4,5,6,7] where equation 3 is satisfied when an energy functional is minimized over a triangular mesh covering the region of interest (see Figures 7 and 8).

Figure 9 shows the elements of a computer algorithm used to obtain the flux plots of Figures 4, 5 and 6 based on the mesh configurations of Figures 7 and 8. In the iteration procedure used to solve equation 4 the H/B characteristic of the iron parts can be modelled in a number of different ways.[18-23]

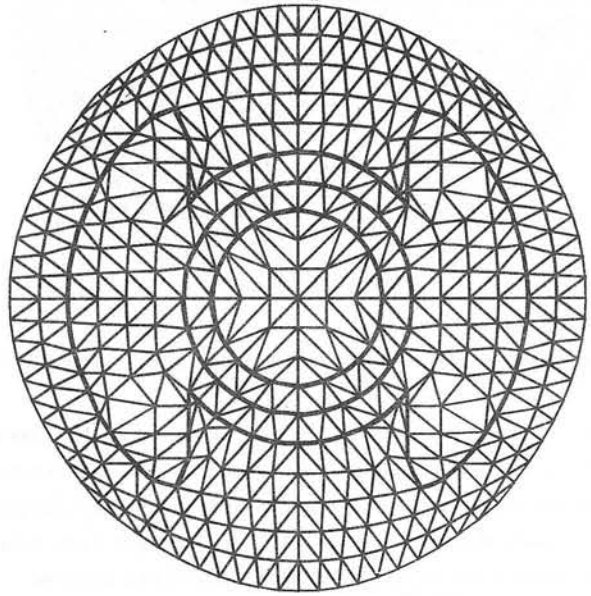

FIGURE 7 Mesh configuration for dc motor flux plot

Application of such an algorithm as a design aid in the construction of electrical machines with p.m. excitation would require modifications to be made depending upon the designers requirements. For example, the prediction of leakage factors might be made by assuming all parts of the magnet to be working at point A in Figure 1. In this case equation 3 is simply modified to include an additional current density term J_m representing the effect of the p.m. material.[24] Prediction of leakage factors after several cycles of operation however, would require accurate knowledge of the demagnetization effects so

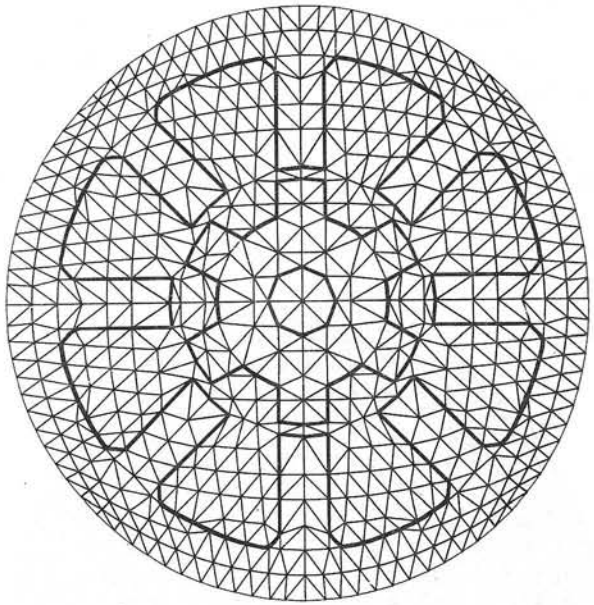

FIGURE 8 Mesh configuration for stepper motor flux plot

that each mesh element within the p.m. material could be characterized correctly. Estimation of leakage reactances in p.m. alternators and stepper motors would also require the development of individual recoil loop models for each element, Some work has already been done on modelling p.m. recoil behaviour by linear approximations and Fröhlich-type equations,[25-27] and perhaps recent work on exponential series representations[28] and phenomenological modelling[29] could be adapted for p.m. machine design.

CONCLUSIONS

The author's purpose in presenting this paper is to indicate some of the areas of p.m. machine design which need additional attention before numerical analysis techniques can be successfully applied. Knowledge of both demagnetization phenomena in electrical machinery and magnetization effects in permanent magnets, coupled with accurate recoil loop modelling techniques will represent a further step towards on-line, interactive design of p.m. structures.

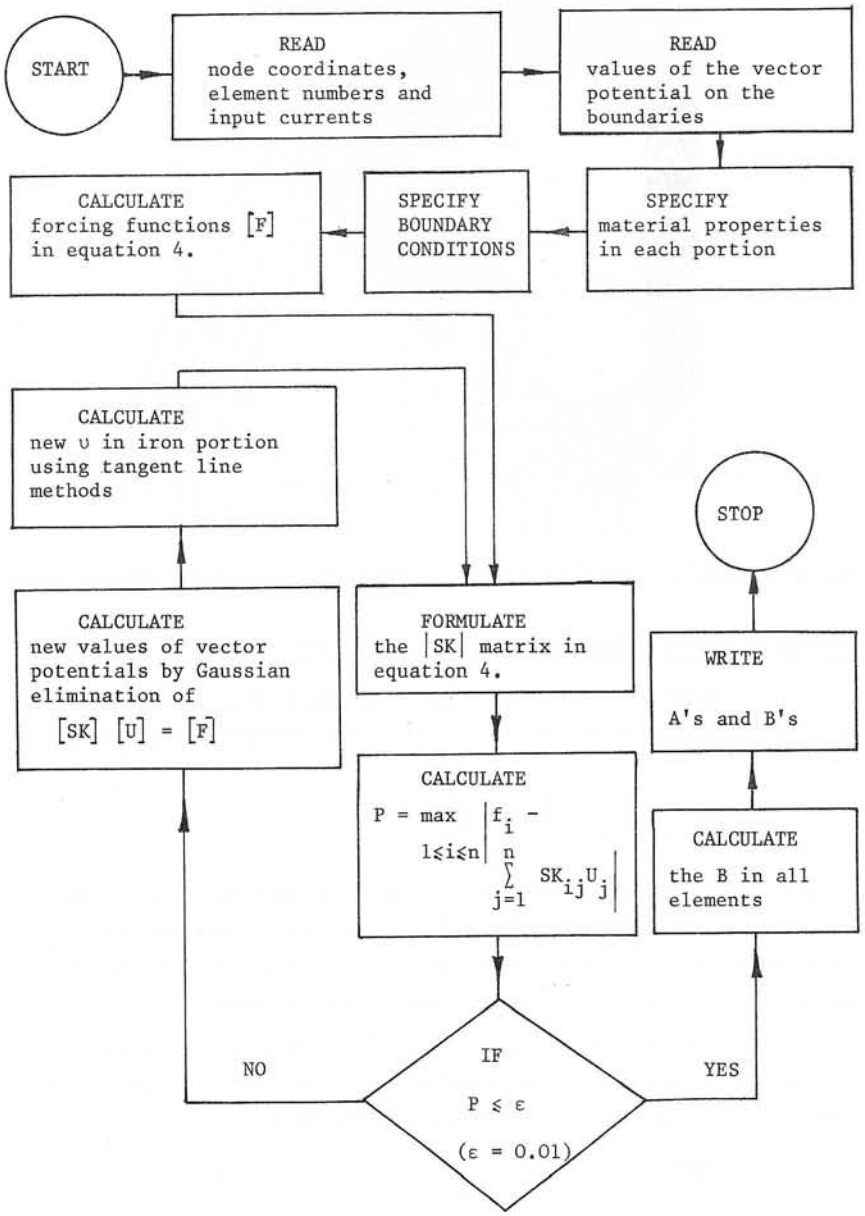

FIGURE 9 Flow chart for finite element program

REFERENCES

1. E.A. ERDELYI, S.V. AHAMED, R.D. BURTNESS, Flux distribution in saturated dc machines at no-load, IEEE Transactions on Power Apparatus and Systems, Vol. 84, May 1965, pp. 375-381.
2. A.M. WINSLOW, Numerical solution of the quasilinear Poisson equation in a nonuniform triangle mesh, Journal of Computational Physics, Vol. 2, 1967, pp. 149-172.
3. E.A. ERDELYI et al., Nonlinear magnetic field analysis of dc machines Parts, I, II, III, IEEE Transactions on Power Apparatus and Systems, Vol. 89, September/October 1970, pp. 1546-1583.
4. M.V.K. CHARI, P. SILVESTER, Finite element analysis of magnetically saturated dc machines, IEEE Transactions on Power Apparatus and Systems, Vol. 90, 1971, pp. 2362-2372.
5. O.W. ANDERSON, Transformer leakage flux program based on the finite element method, IEEE Transactions on Power Apparatus and Systems, Vol. 92, March/April 1973, pp. 682-689.
6. P. SILVESTER, H.S. CABAYAN, B.T. BROWNE, Efficient techniques for finite element analysis of electric machines, IEEE Transactions on Power Apparatus and Systems, Vol. 92, July/August 1973, pp.1274-1281.
7. P. SILVESTER, A. KONRAD, Analysis of transformer leakage phenomena by high-order finite elements, IEEE Transactions on Power Apparatus and Systems, Vol.92, November/December, 1973, pp. 1843-1855.
8. P.Y. HU, Printed circuit motor-disk vs cylinder, Proceedings of the Fourth Annual Symposium on Incremental Motion Control Systems and Devices, University of Illinois, April 1-3, 1975, pp. R.1. - R.8.
9. B.W. WENTWORTH and E.L. ELLIS, Stabilization prediction for permanent-magnet field motors and generators, Journal of Applied Physics, Vol. 37, No.3, March 1966, pp. 1143-1146.
10. Y.S. ZAKHAROV, "The influence of armature reaction on the operation of d.c. motors with permanent magnets", Elektrichestvo, 1958, 78, pp. 34-36.
11. W. LORD, Application of modern p.m. materials to the excitation of a slow-speed servomotor, Journal of Applied Physics, Vol. 37, No.3., March 1966, pp. 1151-1153.
12. W. LORD, Demagnetization phenomena in high-performance dc servomotors, Proc. IEE, Vol. 122, No.4. April 1975, pp.392-294.
13. W. LORD and J.H. HWANG, Leakage field analysis of magnetic circuits by variational methods, Proceedings of the Fourth Annual Symposium on Incremental Motion Control Systems and Devices, University of Illinois, April 1-3, 1975, pp. P1 - P9.
14. V.V. FETISOV, Calculation of commutation reaction in d.c. machines with a brush overlap greater than unity, Elektrichestvo, 1960, 80 pp. 46-50.
15. S. HALASZ, Influence of armature reaction on the stability of d.c. motors, Elektrotechnika, 1963, 56 pp. 157-164.
16. T. ONUKI, A theoretical design of the airgap shape of d.c. machines, Electrotech, J. Japan, 1954, 5 pp. 22-26.
17. D.J. HANRAHAN and D.S. TOFFOLO, Permanent magnet generators - Pt. 2 Optimum design, IEEE Trans. 1963, 82 pp. 68-74.
18. J. FISCHER, H. MOSER, Die Nachbildung von Magnetisierungskurven durch einfache algebraische oder transzendente funktionen, Archiv für Elektrotechnik, Vol. 42, No.5, 1956, pp. 286-299.
19. F.C. TRUTT, E.A. ERDELYI, R.E. HOPKINS, Representation of the magnetization characteristic of dc machines for computer use, IEEE Transactions on Power Apparatus and Systems, Vol. 87, March 1968, pp. 665-669.
20. G.F.T. WIDGER, Representation of magnetisation curves over extensive range by rational-fraction approximations, Proc. IEE, Vol. 116, No.1, January 1969, pp. 156-160.
21. M.K. EL-SHERBINY, Representation of the magnetization characteristic by a sum of exponentials, IEEE Transactions of Magnetics, Vol.9, No.1, March 1973, pp. 60-61.

22. W.K. MACFADYEN, R.R.S. SIMPSON, R.D. SLATER, W.D. WOOD, Representation of magnetisation curves by exponential series, Proc. IEE, Vol. 120, No.8, August, 1973, pp. 902-904.

23. T.S. KRISHNAMOORTHY, M. VENNGOPAL, Determination of best fit parameters of a model for excitation curve, Proceedings of the IEEE, Vol. 61, No.12, December 1973, pp. 1762-1784.

24. K.J. BINNS et al, A rapid method of computation of the magnetic field of permanent magnets, IEEE Transactions on Magnetics, Vol.11, No.5, September 1975, pp. 1538-1540.

25. W.J. HARROLD, Calculation of equipotentials and flux lines in axially symmetrical permanent magnet assemblies by computer, IEEE Transactions of Magnetics, Vol.8, No.1. March 1972, pp.23-29.

26. S.A.Y. SABIR and W. SHEPHERD, Magnetic properties of Alcomax 111 with dynamic excitation, Proc. IEE, Vol. 121, No.8, August 1974, pp. 907-912.

27. J. SLOMCZYNSKA, Nonlinear analysis of the magnetic flux distribution in the magnetized magnet stabilized in air, IEEE Transactions on Magnetics, Vol.10, No.4., December 1974, pp. 1109-1113.

28. J.W. TEAPE et al, Representation of magnetic characteristic, including hysteresis, by exponential series, Proc. IEE, Vol.121, No.9, September 1974, pp. 1019-1020.

29. W.H. DIERKING and C.T. KLEINER, Phenomenological magnetic core model for circuit analysis programs, IEEE Transactions on Magnetics, Vol.8, No.3, September, 1972, pp.594-596.

ACKNOWLEDGEMENTS

The author gratefully acknowledges the assistance of J.H. Hwang of Tuboscope Inc., for producing the flux plots in this paper. He would also like to thank Professor B.C. Kuo of the University of Illinois, for permission to publish Figures 4, 5, 6, 7 and 8.